

Diversity of the Pacific–Japan Pattern among CMIP5 Models: Role of SST Anomalies and Atmospheric Mean Flow

HAINAN GONG, LIN WANG, WEN CHEN, RENGUANG WU, GANG HUANG, AND DEBASHIS NATH

Center for Monsoon System Research and State Key Laboratory of Numerical Modeling for Atmospheric Sciences and Geophysical Fluid Dynamics, Institute of Atmospheric Physics, Chinese Academy of Sciences, Joint Center for Global Change Studies, Beijing, China

(Manuscript received 11 August 2017, in final form 23 May 2018)

ABSTRACT

This study investigates the reproducibility of the spatial structure and amplitude of the observed Pacific–Japan (PJ) pattern in the phase 5 of the Coupled Model Intercomparison Project (CMIP5) models. In particular, the role of sea surface temperature anomalies (SSTAs) and atmospheric mean flow in the diverse reproducibility of the PJ pattern among models is investigated. Based on the pattern correlation between simulated and observed PJ patterns, models are categorized into high and low correlation groups, referred to as HCG and LCG, respectively. The observed cold SSTAs in the western North Pacific (WNP) and equatorial central Pacific, organized convection and precipitation anomalies, and Rossby wave response are reproduced well in HCG models, whereas these features are not present in LCG models. The summer SSTAs are closely tied to the preceding El Niño–Southern Oscillation and its temporal evolution in the tropical Indo-Pacific Ocean in both observations and models, but the SSTAs in the Indian Ocean are weak in both HCG and LCG, implying a weak Indian Ocean capacitor effect. As a result, the reproducibility of the amplitude of the WNP center of the PJ pattern is mainly modulated by the SSTAs and local air–sea feedback over the WNP in the models. On the other hand, a model with stronger climatological southerly along the coast of East Asia tends to produce more realistic amplitude of the midlatitude center of the PJ pattern with clearer poleward wave-activity fluxes due to more efficient local barotropic energy conversion from the mean flow.

1. Introduction

The Pacific–Japan (PJ) pattern, also known as the East Asian–Pacific (EAP) pattern, is one of the important teleconnection patterns affecting the summertime climate anomaly over the East Asia–western North Pacific area (EA–WNP) (Nitta 1987; Huang and Sun 1992; Kosaka and Nakamura 2006; Huang et al. 2012; Li et al. 2014; Wang et al. 2016; Xu et al. 2018, manuscript submitted to *J. Climate*). The PJ pattern is characterized by a meridional wave train in the lower troposphere triggered by anomalous convection over the Philippine Sea (Nitta 1987; Huang and Sun 1992), which can be successfully simulated with imposed diabatic heating based on a two-layer atmospheric model (Kosaka and Nakamura 2010). It is also believed that the PJ pattern describes the covariations of the East Asian summer monsoon (EASM) and the western North Pacific summer monsoon (WNPSM) with opposite circulation anomaly over EA and the WNP (e.g., Wu and Wang

2002; Lee et al. 2006; Gao et al. 2011; Chowdary et al. 2013; Srinivas et al. 2018).

Many studies demonstrated that the lower-tropospheric anomalous circulation and the convective activity over the WNP are largely forced by sea surface temperature anomalies (SSTAs) (e.g., Wang et al. 2001; Lu et al. 2006; Yang et al. 2008; Xie et al. 2009; Li et al. 2012; Zhao et al. 2015; Z. Chen et al. 2016; Chen et al. 2017; Li et al. 2016, 2017; Zhang et al. 2017). Given realistic tropical sea surface temperature (SST) forcing, the PJ pattern is largely captured in either the atmospheric model or the partially coupled model, especially over the tropics (Chen and Zhou 2014; Ding et al. 2014). However, the PJ pattern is not a pure SST-forced mode because the formation and maintenance of the PJ pattern involve interactions between eddy and mean flow, especially in the middle and high latitudes (Kosaka and Nakamura 2006). Thus, the state of the atmospheric mean flow may also play an important role in the formation of the PJ pattern.

Climate models are an essential tool to study the mechanism of climate variability. It is important to understand the capacity and uncertainty of climate models

Corresponding author: Dr. Lin Wang, wanglin@mail.iap.ac.cn

DOI: 10.1175/JCLI-D-17-0541.1

© 2018 American Meteorological Society. For information regarding reuse of this content and general copyright information, consult the [AMS Copyright Policy](https://www.ametsoc.org/PUBSReuseLicenses) (www.ametsoc.org/PUBSReuseLicenses).

to reproduce the observed PJ pattern. Kosaka and Nakamura (2011) reported that the observed PJ pattern can be roughly captured in most climate models, but the intermodel spread of the simulated PJ pattern is still large. Recently, the outputs from phase 5 of the Coupled Model Intercomparison Project (CMIP5) models have been released (Taylor et al. 2012). Compared with the earlier phase 3 (CMIP3), CMIP5 models have higher resolution and more complete representation of the Earth system (Taylor et al. 2012). The outputs of CMIP5 models provide a good opportunity to investigate the reproducibility of the latest state-of-the-art climate models in simulating the observed PJ pattern. Although some studies have analyzed the WNP anomalous anticyclone in CMIP5 models (e.g., He and Zhou 2014; Song and Zhou 2014a; Tao et al. 2016; Ramu et al. 2018), limited study has been carried out to investigate the model's reproducibility of the spatial structure and amplitudes in the observed PJ pattern in CMIP5 models. Meanwhile, the roles of SST anomalies and mean flow on the diverse reproducibility of the observed PJ pattern in CMIP5 models have not been explored yet. Since the diverse abilities of models in reproducing the observed PJ pattern largely reflect the internal variability of climate system, the investigation of the reasons responsible for the diverse model PJ patterns in climate models may provide insights into plausible reasons for the observed interdecadal change in the PJ pattern, which had been attributed to the internal variability of climate system (Xie et al. 2010; Chowdary et al. 2012; Kubota et al. 2016).

Based on the outputs from 36 CMIP5 CGCMs, this study attempts to address these questions: How well do the CMIP5 models reproduce the observed PJ pattern including its spatial structure and the amplitudes? What are the possible origins of the diversity in the model's reproducibility of the observed PJ pattern, and what roles do the SST anomalies and mean flow play to induce this diversity? The rest of this study is organized as follows. Section 2 describes the data and methods. Section 3 presents the origins of the diversity of the reproducibility in the spatial structure of the observed PJ pattern in CMIP5 models. Section 4 analyzes the origins of the diversity of the reproducibility in the amplitude of the observed PJ pattern in CMIP5 models. Finally, the summary and discussion are presented in section 5.

2. Data and methods

a. Data

In this study, the observational proxies of the atmospheric variables are from the monthly mean data of the European Centre for Medium-Range Weather Forecasts (ECMWF) interim reanalysis (ERA-Interim)

dataset, which spans the period January 1979 to present with a $2.5^\circ \times 2.5^\circ$ horizontal resolution (Dee et al. 2011). The monthly SST data used in this study are from the Extended Reconstructed SST version 3 (ERSST v3) dataset (Smith et al. 2008), which has a horizontal resolution of $2^\circ \times 2^\circ$ and covers the period from January 1854 to the present. The monthly outgoing longwave radiation (OLR) data are from National Oceanic and Atmospheric Administration (NOAA) interpolated outgoing longwave radiation on a $2.5^\circ \times 2.5^\circ$ grid (Liebmann and Smith 1996). The Global Precipitation Climatology Project (GPCP) monthly data, with $2.5^\circ \times 2.5^\circ$ resolution, cover the period from January 1979 to the present (Huffman et al. 2009).

b. Models

The first realizations of the historical experiments from 36 CMIP5 CGCMs are analyzed in this study (Taylor et al. 2012). They are ACCESS1.0, ACCESS1.3, BCC-CSM1.1, BCC-CSM1.1(M), BNU-ESM, CanESM2, CCSM4, CESM1-BGC, CESM1-CAM5, CESM1-FASTCHEM, CESM1-WACCM, CMCC-CM, CNRM-CM5, CSIRO-Mk3.6.0, FGOALS-g2, FIO-ESM, GFDL-CM2.1, GFDL-ESM2G, GFDL-ESM2M, GISS-E2-H, GISS-E2-R, HadCM3, HadGEM2-AO, HadGEM2-CC, HadGEM2-ES, INM-CM4, IPSL-CM5A-LR, IPSL-CM5B-LR, MIROC4h, MIROC-ESM, MIROC-ESM-CHEM, MPI-ESM-LR, MPI-ESM-MR, MPI-ESM-P, MRI-CGCM3, NorESM1-M. See <http://cmip-pcmdi.llnl.gov/cmip5/availability.html> for details. To compare the model results with observations, the atmospheric variables, OLR, and precipitation from model outputs have been bilinearly interpolated to a resolution of $2.5^\circ \times 2.5^\circ$, and the SST data from model outputs have been interpolated to a resolution of $2^\circ \times 2^\circ$.

c. Analysis methods

The PJ pattern is the dominant low-frequency anomaly pattern over the summertime WNP in observations. It can be well extracted by the dominant mode of the 850-hPa vorticity field over the domain of 0° – 60° N, 100° – 160° E based on the empirical orthogonal function (EOF) analysis (Kosaka and Nakamura 2010). To investigate the model's reproducibility of the observed dominant mode over the WNP, that is, the observed PJ pattern, the leading modes of the 850-hPa vorticity field over the domain of 0° – 60° N, 100° – 160° E in models are extracted to represent the model PJ pattern (Kosaka and Nakamura 2011). It should be pointed out that the leading modes in models may differ from the observed PJ pattern. For convenience, hereafter they are called the model PJ pattern in this study. Meanwhile, it is noted that in some of the models, EOF1 is not well separated from EOF2 according to the criteria of

North et al. (1982). In some models, EOF1 has a higher pattern correlation, whereas in other models EOF2 has a higher pattern correlation with the observed PJ pattern. Therefore, following Kosaka and Nakamura (2011), the model PJ pattern is defined as a linear combination of EOF1 and EOF2 for a given CMIP5 model as

$$\zeta' = (\zeta'_1 \sqrt{\lambda_1} \cos \theta + \zeta'_2 \sqrt{\lambda_2} \sin \theta) / \sqrt{\lambda_1 \cos^2 \theta + \lambda_2 \sin^2 \theta}. \quad (1)$$

Here, ζ' is the PJ pattern in the model 850-hPa vorticity field; ζ'_1 and ζ'_2 denote 850-hPa vorticity anomalies associated with EOF1 and EOF2 in the model, respectively; and λ_1 and λ_2 are the corresponding eigenvalues. In (1), θ is determined so that the pattern correlation of ζ' with the observed PJ pattern maximizes. In practice, the best value of θ in (1) is determined by evaluating the pattern correlation for 1° intervals of θ for each of the models (Kosaka and Nakamura 2011). The PJ index is constructed by projecting the 850-hPa vorticity anomalies onto the model PJ pattern (ζ'). It is noted that if the model PJ pattern is simply defined as the EOF1 or EOF2 that has a higher correlation to observed PJ pattern, the results remain almost the same as those reported in this study (figures not shown). In addition, the wave-activity flux is used to delineate the propagation of the stationary Rossby waves (Takaya and Nakamura 2001). The boreal winter Niño-3.4 index defined as the averaged SSTA over the domain of 5°S – 5°N , 120° – 170°W was employed to represent El Niño–Southern Oscillation (ENSO).

The multimodel ensemble (MME) was calculated by averaging the variables in all the models with equal weighting. The MME of a regression pattern was calculated as the equally weighted average of corresponding patterns in all the models. Following our previous studies (Gong et al. 2014, 2015; H. Gong et al. 2017; Wang et al. 2018, manuscript submitted to *Climate Dyn.*), the t value averaged over all the models was used to evaluate the confidence level of the MME pattern based on a two-tailed Student's t test. In this study, we mainly focus on the interannual variability. Therefore, all the original data are linearly detrended prior to the analysis, and the boreal summer mean [June–August (JJA)] over 1979–2005 are considered to evaluate the characteristics of interannual PJ pattern.

3. Origins of the diverse spatial structure of the model PJ pattern among CMIP5 models

a. The spatial structure of the model PJ pattern in CMIP5 models

Figures 1a–c show the spatial structure of the PJ teleconnection pattern in the ERA-Interim dataset

(referred to as observations hereafter), which explains about 24% of the total variance in the corresponding domain. A meridional wave train pattern is observed with zonally elongated anticyclonic, cyclonic, and anticyclonic vorticity anomalies in the lower troposphere over the EA-WNP (Figs. 1a,c). The corresponding OLR and precipitation anomalies show meridional tripoles with suppressed convection/precipitation over the WNP and north of Japan and enhanced convection/precipitation extending from the Yangtze River Valley to south of Japan (Figs. 1b,c). The MME reproduces the locations of meridional wave-type anomalies (Fig. 1d) with a pattern correlation coefficient of 0.89 in the vorticity field (0° – 60°N , 100° – 160°E). The magnitude of the model PJ pattern is generally weaker in the MME than in the observations, especially for the center north of Japan (Fig. 1d). This bias was identified in another version climate models reported by Kosaka et al. (2012). The north center of the model PJ pattern is located at middle and high latitudes, and it may be affected by the atmospheric processes such as the Silk Road pattern and the Eurasian pattern (e.g., Nakamura and Fukamachi 2004; Z. Gong et al. 2017). The atmospheric processes in the middle to high latitudes are chaotic and may not be well reproduced by the current models. The model PJ-related OLR and precipitation anomalies over EA-WNP are both weaker in MME than in the observations (Figs. 1e,f). The suppressed convection and precipitation anomalies north of Japan are missing in the MME (Figs. 1e,f). We further calculate the pattern correlation coefficient of the PJ pattern between each model and observations. There is a large spread of pattern correlations among the models with a maximum pattern correlation coefficient of 0.83 and a minimum pattern correlation coefficient of only 0.4 (Fig. 1g). This suggests that the capacity in reproducing the spatial structure of the observed PJ pattern varies largely among CMIP5 models.

To further illustrate the differences in the reproducibility of the spatial structure of the observed PJ pattern among models, the six models with the highest and lowest correlation are selected based on the pattern correlation coefficient between models and observations. The results of the MME in the high pattern correlation models group (HCG) and low pattern correlation models group (LCG) are shown in Fig. 2. The HCG models well reproduce the spatial structure of the observed PJ pattern with meridional wave-type anomalies (Fig. 2a), similar to that in observations. Meanwhile, the related OLR and precipitation anomalies over the EA-WNP are also well captured in HCG models except for the center north of Japan, which is

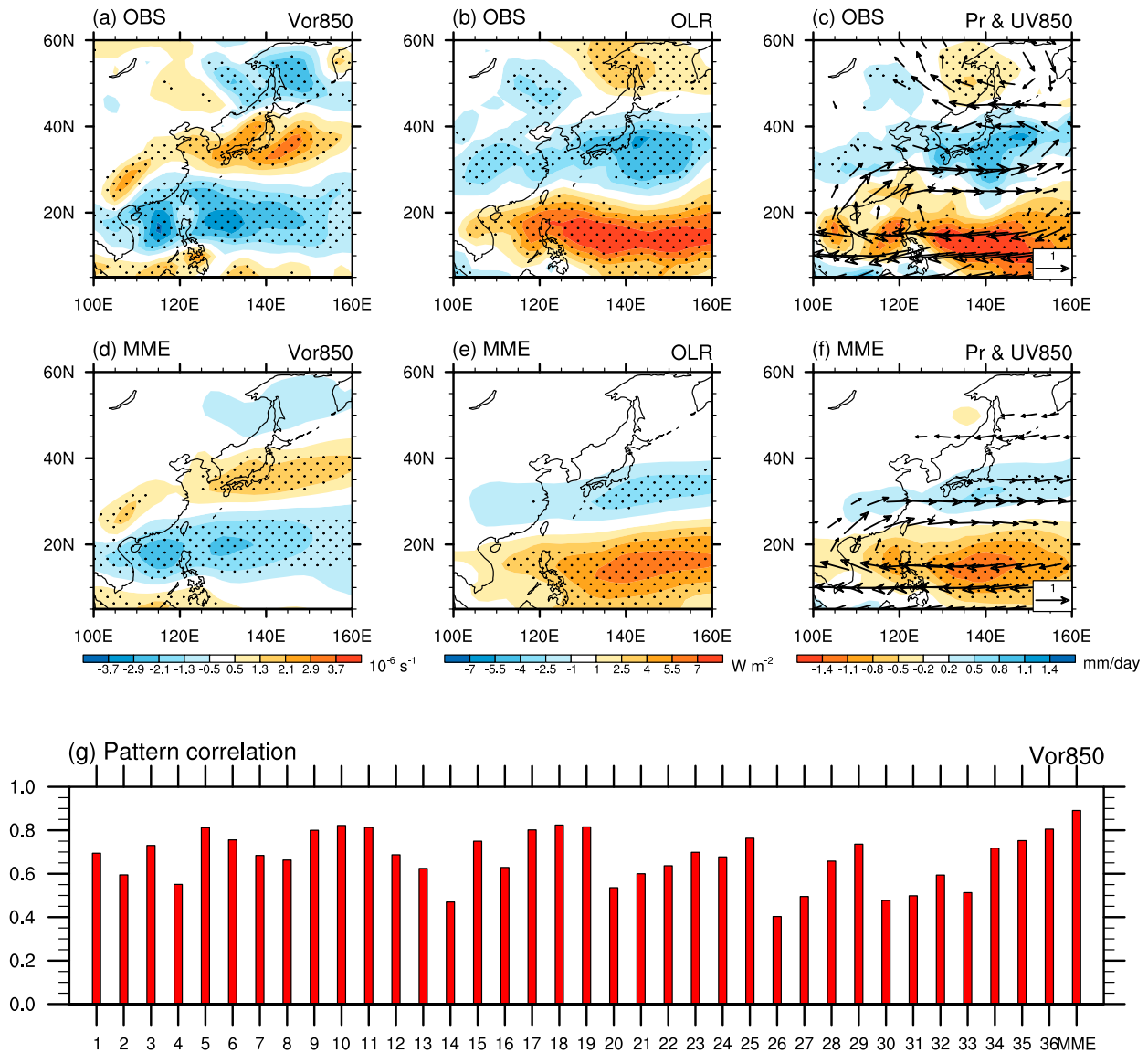


FIG. 1. The JJA mean (a) 850-hPa vorticity, (b) OLR, and (c) precipitation (shading) and 850-hPa wind (vector) anomalies regressed onto the normalized PJ index during 1979–2005 in observations. (d)–(f) As in (a)–(c), but for MME of 36 CMIP5 models. (g) The pattern correlation coefficient of 850-hPa vorticity anomalies over EA–WNP (0° – 60° N, 100° – 160° E) between models and observations. Dots in (a)–(f) indicate that the anomalies are significant at the 90% confidence level based on a two-sided Student's t test.

weaker than in observations (Figs. 2a–c). In contrast, in LCG models, vorticity anomalies over the EA–WNP are much weaker, especially for the center over the WNP (Fig. 2d). Moreover, the centers of convective and precipitation anomalies over the WNP are very weak and shift southward in LCG models compared to observations (Figs. 2e,f). It is noted that although the model PJ-related anomalies in individual LCG models are not fully consistent with the MME, the major features are the same. These results confirm that there are large intermodel spreads in reproducibility of the spatial

structure of the observed PJ pattern among CMIP5 models.

b. Role of simultaneous tropical SST anomalies

The convection anomaly over the WNP as a trigger for the formation of the PJ pattern is largely forced by simultaneous tropical SSTAs in observations (e.g., Kosaka and Nakamura 2006; Chen and Zhou 2014). However, since the responses of atmosphere to SST forcing vary among different models, it is unclear whether there is a certain relationship between the

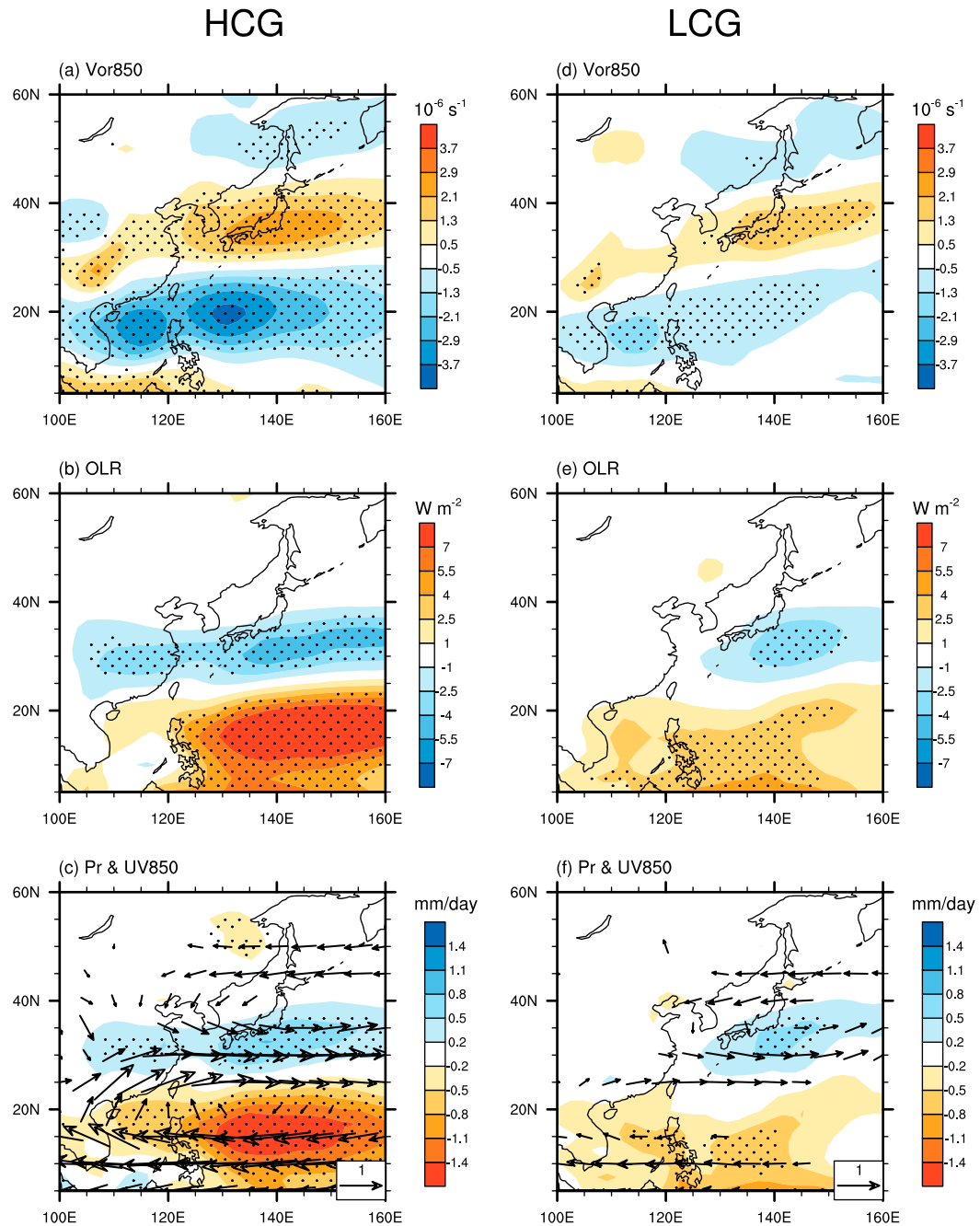


FIG. 2. (a)–(c) As in Figs. 1a–c, but for the MME of six HCG models. (d)–(f) As in (a)–(c), but for MME of six LCG models. Dots indicate that the anomalies are significant at the 90% confidence level based on a two-sided Student's t test.

SSTAs and the responses of the model PJ pattern among models. Therefore, we first examine whether the model's reproducibility of the spatial structure of the observed PJ pattern is related to the simultaneous SSTa pattern in CMIP5 models. In observations, during the positive phases of the PJ pattern, the SSTAs are positive in the entire tropical Indian Ocean (TIO) (Fig. 3a).

Responding to the TIO warming, the anticyclonic vorticity anomaly is generated along with the suppressed convection over the WNP (Figs. 3a,d) due to the atmospheric Kelvin wave response to anomalous heating induced by positive SSTAs in the TIO (Yang et al. 2007; Xie et al. 2009, 2016; Chowdary et al. 2011). Meanwhile, there are cold SSTAs in the equatorial central Pacific

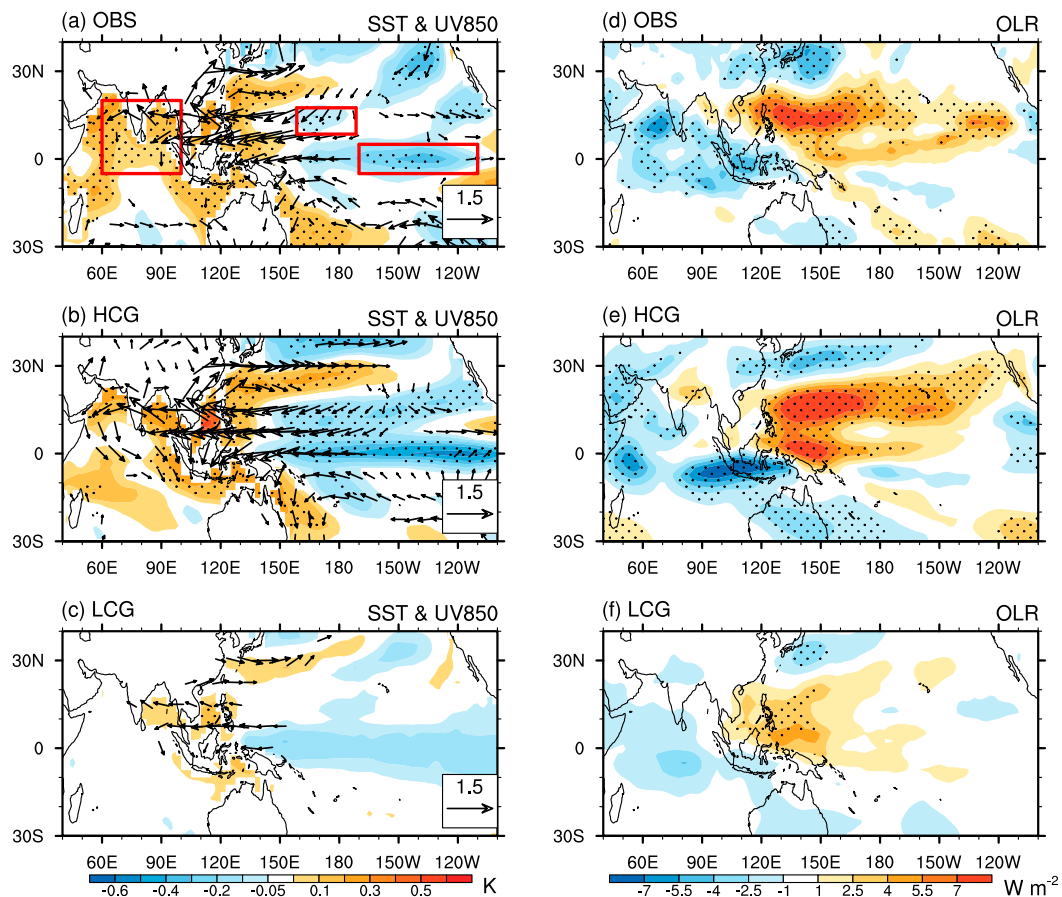


FIG. 3. The simultaneous SST (shading, unit: K) and 850-hPa wind (vectors, unit: m s^{-1}) anomalies regressed onto the normalized PJ index in (a) observations, (b) HCG models, and (c) LCG models. (d)–(f) As in (a)–(c), except for OLR anomalies. Dots indicate that the anomalies are significant at the 90% confidence level based on a two-sided Student's t test.

(Fig. 3a). The central Pacific cooling shifts the rising limb of the Walker cell westward, thus reducing convection around 150°E and increasing convection over the Maritime Continent and tropical eastern Indian Ocean (Fig. 3d). The suppressed convection directly strengthens the anticyclonic vorticity anomaly over the WNP by emanation of descending Rossby waves (Wang et al. 2013; Xiang et al. 2013).

In addition, there are significant cold SSTAs in the WNP around 7.5° – 17.5°N , 160°E – 170°W (Fig. 3a). These SSTAs may play a very important role in maintaining anomalous convection and anomalous anticyclone over the WNP (e.g., Zhang et al. 1996; Wang et al. 2000, 2003; Wu et al. 2010; Jiang et al. 2013; Wang et al. 2013; Wu et al. 2014). Under the mean easterly winds east of 160°E and large mean specific humidity in boreal summer over the WNP, the atmospheric response is sensitive to the SST forcing. These cold SSTAs, though not large, trigger a descending Rossby waves with suppressed convective heating over the WNP, hence establishing a

positive local air–sea feedback (e.g., Xiang et al. 2013). Therefore, the organized convection anomaly over the WNP forced by the SSTAs in tropical Indo-Pacific Ocean (TIP) triggers the meridional teleconnection wave train, forming the PJ pattern (Fig. 3d).

The significant cold SSTAs in the central Pacific and WNP are well reproduced in the HCG models (Fig. 3b). In comparison, the domain of cold SSTAs in the WNP is larger and merged to the cold SSTAs in the central Pacific. Accordingly, anomalous anticyclone over the WNP are well captured in HCG models (Figs. 3b,e). Meanwhile, warm SSTA and convection anomaly over the TIO are much weaker in HCG models compared to observations (Fig. 3b). As such, the effect of TIO on the convection and circulation anomaly over the WNP is weak in HCG models. In contrast, in the LCG models, warm (cold) SSTAs are absent in the TIO (WNP), and the cold SSTAs in the central Pacific are much weaker and insignificant compared to observations (Fig. 3c). Consequently, the

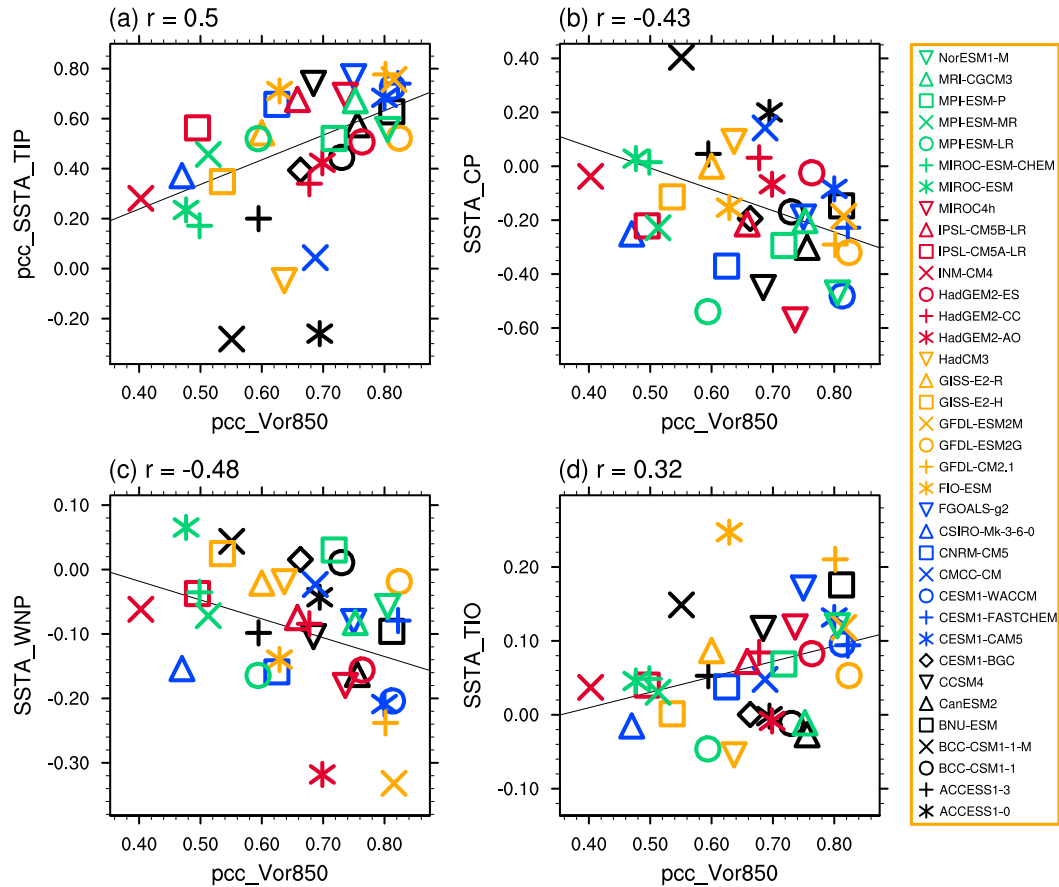


FIG. 4. Scatterplot of the pattern correlation coefficients of 850-hPa vorticity anomalies (x -axis) over EA-WNP (0° – 60° N, 100° – 160° E) between each model and observations with (a) the pattern correlation coefficients of simultaneous SST anomalies (y -axis) over tropical Indo-Pacific (10° S– 25° N, 50° E– 110° W) between each model and observations, (b) the magnitudes of SST anomalies (units: K, y -axis) averaged over tropical central Pacific (5° S– 5° N, 110° – 170° W) in each model (-0.16 K in observations). (c), (d) As in (b), but for the western North Pacific (WNP; 7.5° – 17.5° N, 160° E– 170° W) and tropical Indian Ocean (TIO; 5° S– 20° N, 60° – 100° E), and the observed SST anomalies in WNP and TIO are -0.06 and 0.11 K, respectively.

convection anomaly is weak and unorganized over the WNP (Figs. 3c,f), and thereby the model PJ teleconnection pattern is weak. The weak SSTAs in the TIO in both HCG and LCG models imply a weak Indian Ocean capacitor effect in the models (Xie et al. 2009). Although the TIO SST anomalies in the HCG models are somewhat weaker than that in observations, the warming of SST in the HCG models is much stronger than that in the LCG models. It indicates that the TIO still plays a certain role in the formation of the PJ pattern in models although its effect is weaker than that in observations.

The above results indicate that the SSTA pattern in the TIP plays a key role in the development of anomalous convection over the WNP and thereby the reproducibility of the observed PJ pattern in the models. To support this point of view, we have examined the pattern correlation of SSTAs in the TIP (10° S– 25° N,

50° E– 110° W) between models and observations. The results show that a higher similarity of SSTA distribution in the TIP tends to be accompanied by a more realistic PJ pattern in the models (Fig. 4a). The correlation coefficient between the pattern correlation of SSTA in the TIP and the pattern correlation of vorticity anomalies over the EA-WNP is 0.5, exceeding the 99% confidence level. To further delineate the relative roles of SSTAs in different regions in the model's reproducibility of the spatial structure of the observed PJ pattern, three key areas of SSTAs—the central Pacific (5° S– 5° N, 170° – 110° W), WNP (7.5° – 17.5° N, 160° E– 170° W), and TIO (5° S– 20° N, 60° – 100° E)—are selected (see the red boxes in Fig. 3). Here, we note that the area-mean SSTAs in the specified regions may represent the bias from observations of the model simulated SSTAs in either the spatial distribution or the amplitude. In the case

of difference in the spatial structure, it indicates a shift in the location of SST forcing, which in turn leads to a shift in the model PJ pattern compared with observations.

It is clearly seen that a larger cold SSTA in both the central Pacific and WNP tends to reproduce a more realistic PJ pattern in the models, with the correlation coefficients between the SSTA in the central Pacific and WNP and the pattern correlation of vorticity anomalies over the EA-WNP at -0.43 and -0.48 , respectively, both exceeding the 99% confidence level (Figs. 4b,c). It suggests that the SSTAs in the central Pacific and WNP play an equivalent role in the reproducibility of the spatial structure of the observed PJ pattern in the models. The magnitude of SSTAs in the TIO is generally small compared to that in the central Pacific and WNP in the models. The intermodel relationship of the model PJ pattern with TIO SSTA is also weaker than that with central Pacific and WNP SSTAs in the models, with intermodel correlation coefficient of 0.32 (Fig. 4d). These results suggest that the model's reproducibility of spatial structure of the observed PJ pattern is closely tied to the cold SSTAs in the central Pacific and WNP, whereas there are weak impacts of TIO SSTAs in the models. This result is somewhat different from that in observations because the TIO plays an important role in the formation of the observed PJ pattern. Previous studies indicate that the atmospheric response may be more sensitive to the western Pacific SSTAs than to the TIO SSTAs in climate models (Barsugli and Sardeshmukh 2002; Chen and Zhou 2014). Therefore, this relative weak effect of TIO SSTAs on the model PJ pattern may be related to the different sensitivity of atmospheric responses to SSTAs in the tropical Pacific and the TIO in models.

The precipitation variability related to the PJ pattern is crucial for the summertime flood and drought in the countries in the EA-WNP region (e.g., Zhang et al. 1999). Therefore, we further examine the SSTA pattern in the TIP in relation to the model PJ-related precipitation anomalies over the EA-WNP (Fig. 5). The results are similar to those in the model PJ pattern, but with a higher linear correlation between the simulated precipitation pattern and the SSTA in the TIP. The models with closer resemblance of SSTA distribution in the TIP to observations tends to reproduce a more realistic precipitation anomaly pattern over the EA-WNP (Fig. 5a). Similarly, the precipitation anomaly pattern over the EA-WNP is tightly related to the cold SSTAs in the central Pacific and WNP, with intermodel correlation coefficients of 0.57 and 0.56 , respectively, both of which exceed the 99% confidence level (Figs. 5b,c). But the intermodel correlation coefficient between the precipitation anomaly pattern over the EA-WNP and the

warm SSTAs in the TIO is very weak ($r = 0.34$) (Fig. 5d). This further confirms that the cold SSTAs in the central Pacific and WNP play a more important role than warm SSTA in TIO in the model's reproducibility of the observed precipitation anomaly pattern over the EA-WNP.

c. Role of preceding winter ENSO SSTA

The above results show that the simultaneous SSTAs in the TIP play a key role for the model reproducibility of the observed PJ pattern. Meanwhile, many studies have noted that the summer SSTA in the TIP is largely influenced by the preceding winter SSTA related to ENSO in observations (e.g., Wu et al. 2003; Xie et al. 2009; Yang et al. 1996; Yang and Jiang 2014). Hence, the role of preceding winter tropical SSTA in the reproducibility of the summertime PJ pattern in CMIP5 models is examined. Figure 6 shows the preceding winter SSTA in the TIP regressed on the normalized PJ index in observations and HCG and LCG models. The preceding winter refers to December–February (DJF), denoted as DJF (-1) in Fig. 6. In observations, the SSTAs in DJF related to the summertime PJ pattern show the typical ENSO pattern, in which significant positive SST anomalies are observed over the tropical eastern Pacific (Fig. 6a). In the MME of HCG models, the model PJ-related preceding winter SSTA pattern resembles quite well the observed ENSO pattern, while the magnitude of the SSTA is somewhat smaller than that in observations (Fig. 6b). However, the LCG models fail to reproduce the observed ENSO-like SSTA pattern in the preceding winter associated with the model PJ pattern. Meanwhile, the SSTAs in the TIO are very weak, and the SSTAs in the equatorial central-western Pacific are even negative in the LCG models (Fig. 6c). This implies that the simulation of the relationship between preceding ENSO and PJ variability is very important for the reproducibility of the spatial structure of the observed PJ pattern in the models.

Some previous studies have demonstrated that the simulation of ENSO is important for the reproducibility of the relationship between ENSO and the East Asian monsoon in CMIP5 models (Gong et al. 2015; Song and Zhou 2014b; Jiang et al. 2017). Hence, a question arises: Is the spatial structure of the model PJ pattern tied to the preceding ENSO pattern in the models? To answer this question, the intermodel relationship of the model PJ pattern with the simulated ENSO SSTA pattern among models is shown in Fig. 7a. Here, the ENSO SSTA pattern is defined as the SSTA over the tropical and subtropical Pacific (20°S – 20°N , 130°E – 70°W) regressed against the normalized Niño-3.4 index. The pattern correlation coefficients between models and observations are employed

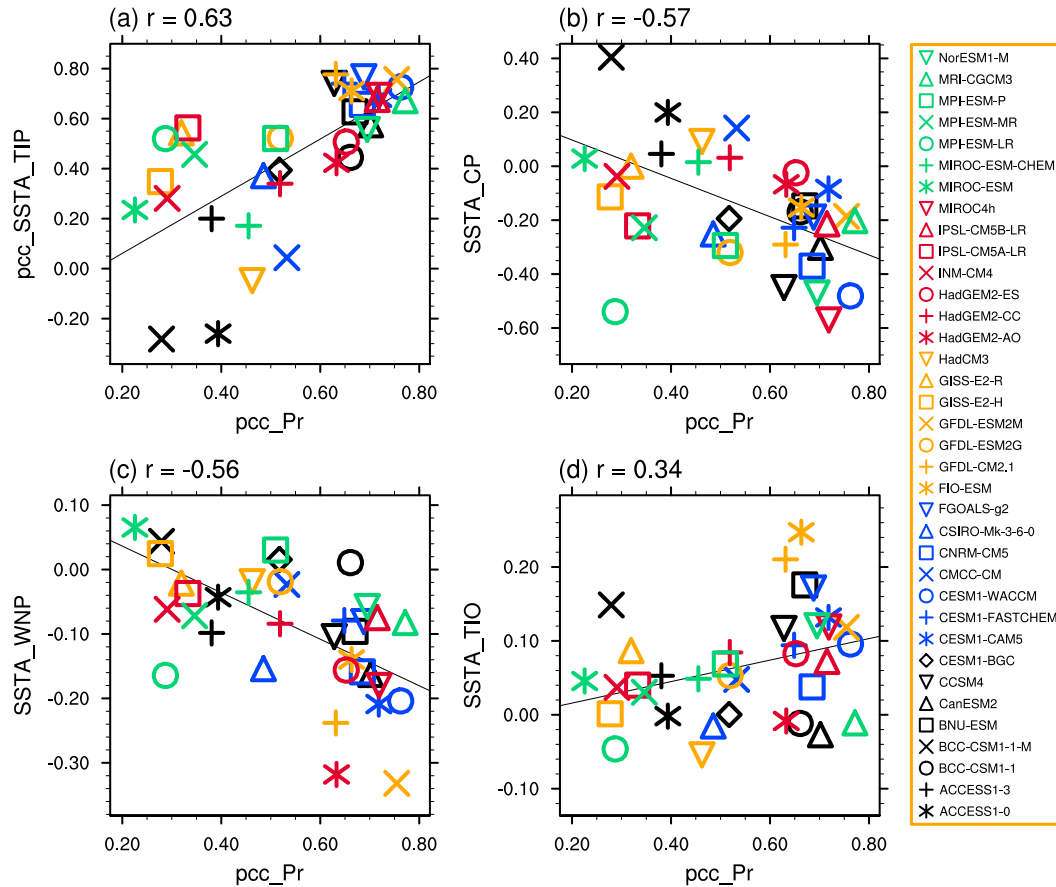


FIG. 5. As in Fig. 4, but for the pattern correlation of precipitation anomalies (x axis) over EA-WNP (0°–60°N, 100°–160°E) between each model and observations.

to represent the capacity of models in reproducing the observed PJ and ENSO SSTA patterns. It can be clearly seen that the models with a good performance in simulating ENSO SSTA pattern in preceding winter tends to reproduce a realistic PJ pattern, with the intermodel correlation coefficient of 0.64, exceeding the 99.9% confidence level (Fig. 7a). It suggests that the simulation of ENSO is crucial for the reproducibility of the spatial structure of the observed PJ pattern in models.

To confirm the above result, six models with the best (or worst) performance in simulating ENSO SSTA pattern are selected based on the pattern correlation coefficient between models and observations. The model PJ pattern in high pattern correlation models (HPCC) is displayed in Fig. 7b. The model PJ pattern is quite similar to that in observations, with a pronounced meridional tripole pattern of zonally elongated vorticity anomalies over the EA-WNP. In contrast, the model PJ pattern is much weaker and unorganized in the low pattern correlation models (LPCC) (Fig. 7c). This result confirms that the reproducibility of the observed PJ

pattern is closely tied to the reproducibility of preceding winter ENSO pattern in models. It is also noted that half the models (three out of six) in HCG are also in HPCC, and five out of six models in LCG are also in LPCC (Fig. 7a).

Furthermore, the SST, precipitation, and circulation anomalies over the TIP in HPCC and LPCC are shown in Fig. 8. It can be seen that in the HPCC models there is significant warming in the TIO and cooling in the central Pacific and WNP (Fig. 8a), similar to observations. The large-scale warming of the TIO in the decaying phase of El Niño could excite a Kelvin wave over the western Pacific, suppressing convection and generating anomalous anticyclonic vorticity over the WNP (Figs. 8a,c). Meanwhile, the cold SSTAs in the central Pacific and WNP suppress the convection over the WNP and directly strengthen the anticyclonic vorticity by exciting descending Rossby waves. Therefore, the organized convection anomaly over the WNP triggers a reasonable PJ pattern over the EA-WNP in HPCC models (Fig. 8c). In contrast, there are no significant SSTAs in

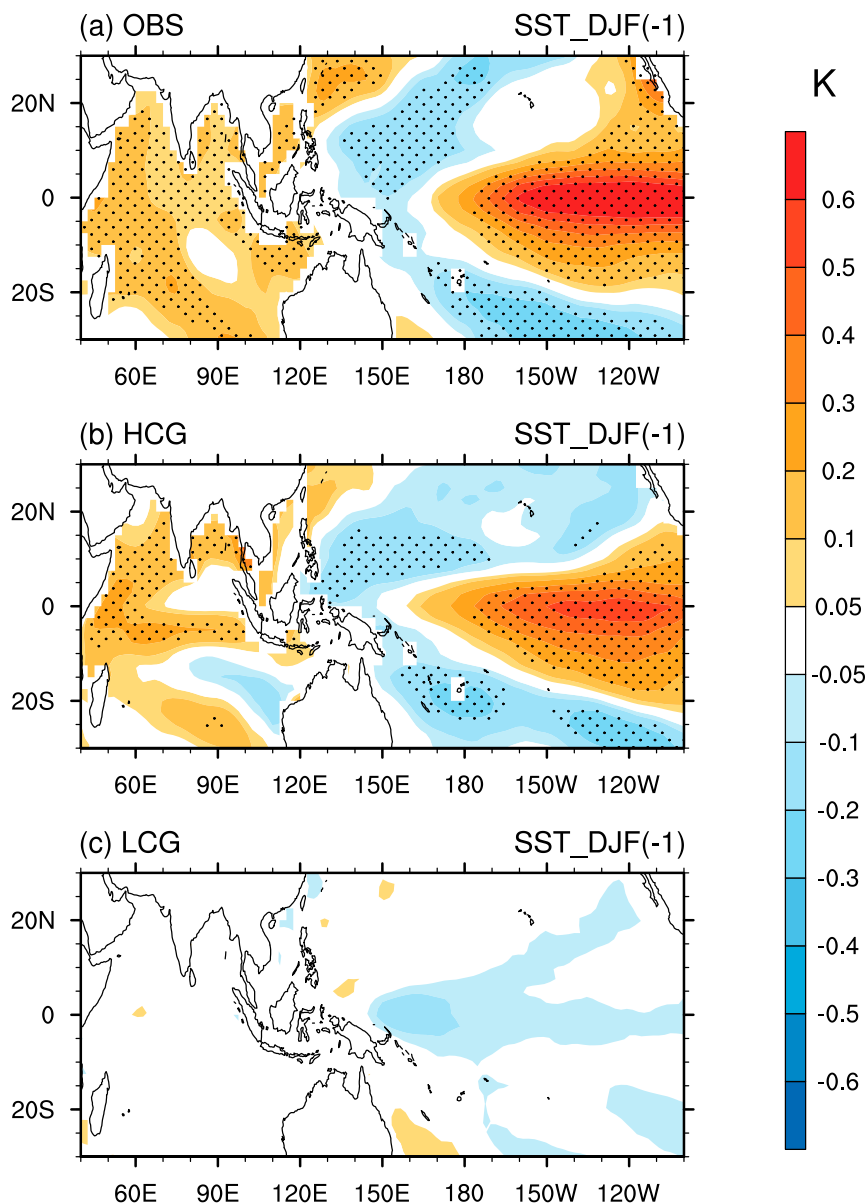


FIG. 6. The SST anomalies in the preceding winter (DJF) regressed on the normalized PJ index in the (a) observations, (b) HCG models, and (c) LCG models during 1979–2005. Dots indicate that the anomalies are significant at the 90% confidence level based on a two-sided Student's *t* test.

the TIO in LPCC models, and the cold SSTAs in the central Pacific and WNP are very weak and insignificant (Fig. 8b). Therefore, the atmospheric responses to the weak SSTAs in TIP are very weak and unorganized, accounting for the unreliable PJ pattern in LPCC models (Fig. 8d). These results confirm that the capacity of models in simulating the spatial structure of the observed PJ pattern is strongly related to the reproducibility of ENSO SSTA pattern in CMIP5 models.

It is noted that the preceding winter SSTA associated with the PJ pattern displays a typical ENSO pattern in observations, with large-scale warming in the tropical central and eastern Pacific (Fig. 6), whereas the PJ-related simultaneous SSTA is characterized by cooling in the tropical Pacific, especially in equatorial central Pacific. Therefore, the evolution of the ENSO SSTA from preceding winter to concurrent summer may be very important to the formation of the PJ pattern both in observations and models. Figure 9 displays the temporal evolutions of

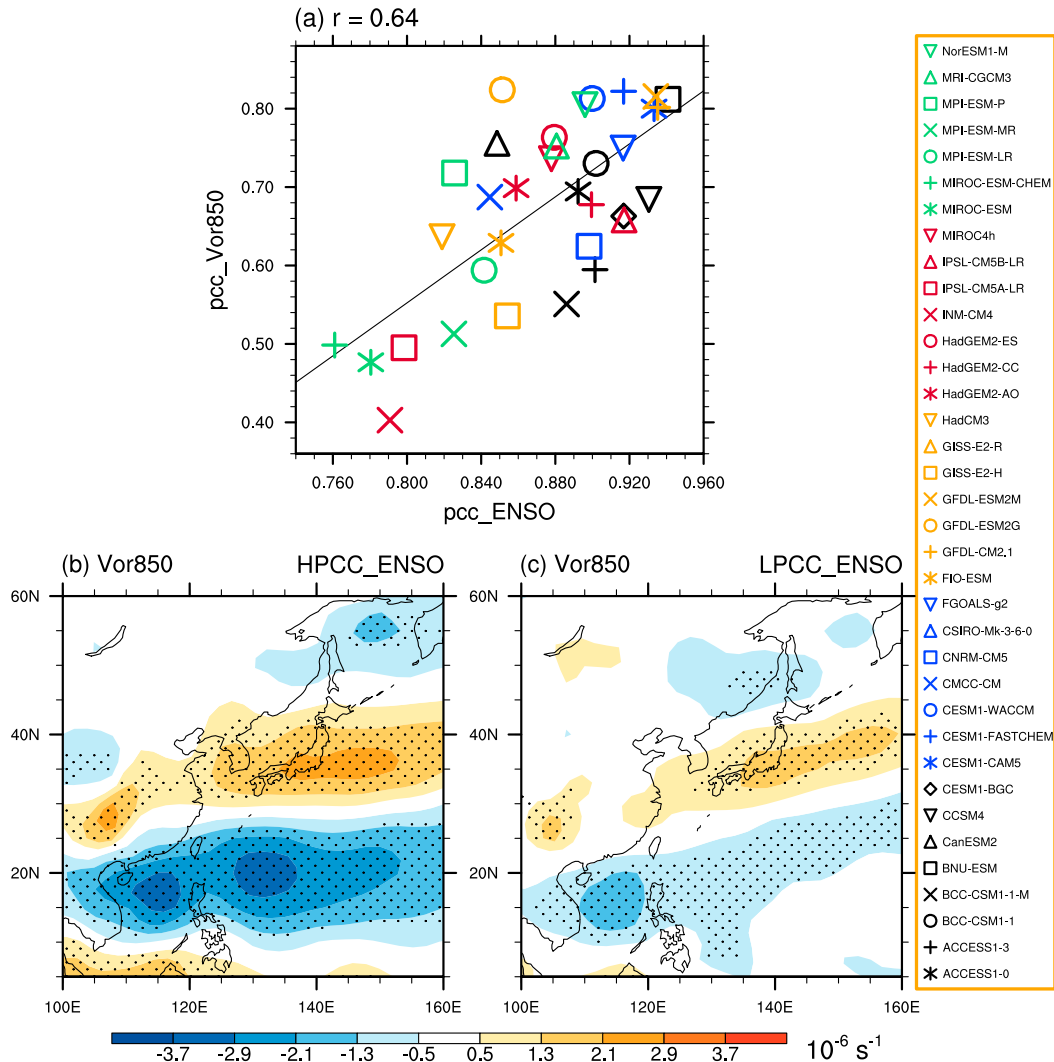


FIG. 7. (a) Scatterplot of the pattern correlation coefficients of the ENSO-related SSTA over the tropical Pacific (20°S – 20°N , 130°E – 70°W) in preceding winter (x axis) vs the PJ-related 850-hPa vorticity anomalies over EA-WNP (0° – 60°N , 100° – 160°E) in summer (y axis) in each model and observations. (b) and (c) are the MME of the PJ pattern represented by 850-hPa vorticity anomaly in the six models with highest (HPCC) and lowest (LPCC) pattern correlation of ENSO SSTA between each model and observations, respectively.

PJ-related SSTAs in the region of 5°S – 5°N , 170°E – 140°W in observations, HPCC models, and LPCC models. The evolution of SSTAs related to the model PJ pattern is quite consistent with observations in the HPCC models, with warm SSTA in preceding winter that gradually weakens and is replaced by cold SSTA in later summer. It actually reflects a fast decaying of an El Niño event and transition to a La Niña event. During such years, the warm SSTA in TIO induced by the preceding El Niño via the atmospheric bridge and the cold SSTA in the central Pacific together trigger the atmospheric anticyclonic responses over the WNP, thereby generating a reasonable PJ teleconnection over the EA-WNP in the HPCC models (Fig. 7b). The

combined effect of opposite SSTAs in the TIO and central Pacific in the atmospheric response over the WNP has been demonstrated using model experiments (Chen et al. 2017).

In contrast, the model PJ-related SSTA in preceding winter features weak cooling that persists to concurrent summer in the LPCC models (Fig. 9). This implies that the model PJ pattern in LPCC models might be related to the developing (or persisting) weak La Niña events. In fact, the ENSO SSTA pattern generally has a westward expansion in CMIP5 models, especially in the LPCC models (figure not shown). The evolutions of ENSO SSTAs in all the LPCC models are slower than that in observations and HPCC models due to the weak damping

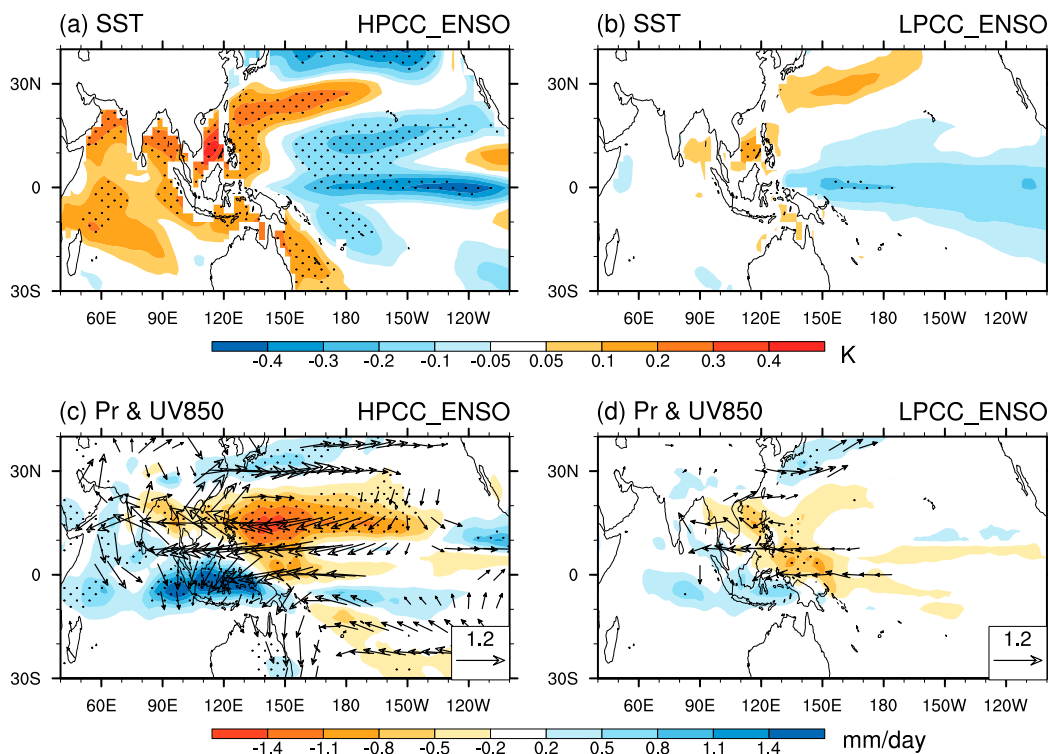


FIG. 8. The simultaneous SST anomalies regressed onto the normalized PJ index in (a) HPCC_ENSO and (b) LPCC_ENSO models. (c),(d) As in (a),(b), but for precipitation (shading) and 850-hPa winds (vectors; unit: m s^{-1}). Dots indicate that the anomalies are significant at the 90% confidence level based on a two-sided Student's t test.

effect (Jiang et al. 2017). Moreover, the weak cold SSTA in preceding winter in tropical Pacific is difficult to reproduce, as is the SSTA in the TIO, so the SSTA in the TIO in summer is almost absent and the cold SSTA in the central Pacific is also very weak (Fig. 8b). The resultant atmospheric responses are very weak and unorganized, leading to unreasonable PJ pattern in LPCC models (Fig. 8d). This result also supports the previous finding that the variations in the decay phases of El Niño are likely to produce large differences in circulation over the WNP region (W. Chen et al. 2016; Chowdary et al. 2017).

The above results confirm that the reproducibility of ENSO SSTA in the preceding winter is important for the reproducibility of the spatial structure of the observed PJ pattern during the ENSO decaying summer in CMIP5 models. The unrealistic ENSO SSTA pattern causes the unreasonable evolution of ENSO SSTA in the decaying summer and thereby induces the unrealistic atmospheric responses over the EA-WNP.

4. Origins of the reproducibility of amplitudes of the observed PJ pattern among CMIP5 models

The pattern correlations can reflect the resemblance of the spatial structure but cannot describe the model's

reproducibility of the intensity of the observed PJ pattern. For example, the pattern correlation between MME and observations is the highest compared with any single model, but the amplitudes of the centers of the PJ pattern in MME are generally weaker than those in HCG models. Therefore, the origins of the model's reproducibility of the amplitudes in the centers of the observed PJ pattern in models need to be further examined. The model's reproducibility of the magnitudes of anomalies in the centers of the observed PJ pattern

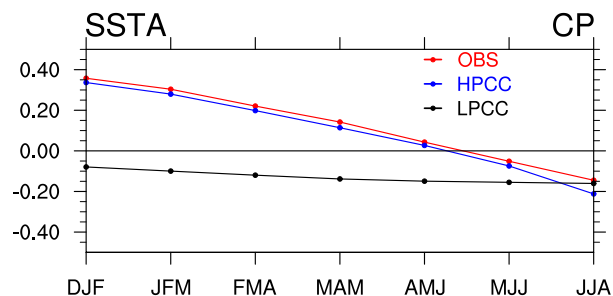


FIG. 9. Temporal evolutions of area-averaged SST anomalies (units: K, y axis) over the tropical central Pacific (5°S – 5°N , 170°E – 140°W) in observations (red line), HPCC_ENSO models (blue line), and LPCC_ENSO (black lines) models during 1979–2005.

may be related to the shift in the spatial structure or the difference in the amplitude of anomalies compared to observations. However, the spatial structures of the model PJ pattern do not show much difference in most of the models from that in observations (figure not shown), and a relatively large difference is only seen in some LCG models. Therefore, the model's reproducibility of the magnitudes of anomalies in the centers of the observed PJ pattern may be learned by comparing area-mean anomalies with observations in most of the models.

a. Role of local air–sea interaction

The lower-level atmospheric circulation over the WNP is tied to anomalous convection over the WNP, which is largely forced by SSTAs in the TIP (e.g., Wang et al. 2001; Wu and Wang 2000; Li and Wang 2005). The cold SSTAs in the central Pacific and WNP together with the warm SSTAs in the TIO can all generate convection and circulation anomalies over the WNP. Therefore, a question arises: Which SSTAs influence the model's reproducibility of the WNP center of the observed PJ pattern among models? Figure 10a presents the intermodel correlation of area-averaged PJ-index regressed 850-hPa vorticity anomalies over the domain 15° – 27.5° N, 110° – 140° E, covering the major regions of large vorticity anomalies over the WNP in the observed PJ pattern, with a simultaneous PJ-index regressed SSTA in the TIP among 36 CMIP5 models. There are significant negative correlations near the WNP center of the observed PJ pattern (Fig. 10a). This indicates that a warmer SSTA tends to correspond to a stronger anomalous anticyclone. It suggests a passive response of SSTA to the atmospheric anomaly in the WNP due to the increasing downward shortwave radiation in the region of the WNP center. Significant positive correlations are found mainly in the Philippine Sea (Fig. 10a). The correlation indicates that anticyclonic anomalies correspond to a colder SSTA. Figure 10c shows the scatter diagram of area-averaged SSTA in the core area (10° – 15° N, 145° – 170° E) denoted as SSTA_WNP with 850-hPa vorticity anomalies in the WNP defined in the previous paragraph. There is a clear linear relationship with the intermodel correlation coefficient of 0.62, exceeding the 99.9% confidence level. This relationship is further confirmed when the vorticity anomalies are replaced by convection anomalies over the WNP (Figs. 10b,d). A positive OLR anomaly corresponds to a negative SSTA, with an intermodel correlation coefficient of -0.54 , exceeding the 99% confidence level (Fig. 10d). The cold SSTA suppresses the in situ convection activity over the WNP, triggering descending Rossby waves that force the anticyclonic anomaly

northwest of cold SSTA. In turn, the anomalous northeasterly winds of the anticyclone strengthen mean easterlies to the east of the monsoon trough, thereby enhancing evaporation and entrainment that reinforces the cold SSTA in the WNP. Hence, there is positive local air–sea feedback in the above region. These results suggest that the reproducibility of the amplitudes of the WNP center in the observed PJ pattern is largely determined by the local air–sea interaction triggered by cold SSTA in the WNP in models.

To further elucidate the role of SSTAs, seven models with SSTA in the WNP less than -0.15 K (cSSTA) and eight models with SSTA in the WNP larger than 0K (wSSTA) are selected for comparison. Figures 10e and 10f display the composite map of the model PJ pattern in the cSSTA and wSSTA models, respectively. It can be clearly seen that the magnitude of the WNP center in cSSTA models is almost twice as large as that in wSSTA models (Figs. 10e,f). This result supports the role of cold SSTA in WNP in modulating the amplitude of the WNP center through a positive thermodynamic air–sea feedback in models. In other words, the local air–sea interaction over the WNP can significantly influence the reproducibility of the amplitude of the WNP center in CMIP5 models. Moreover, the magnitudes of the EA center of the PJ pattern are close to each other in cSSTA and wSSTA models, both of which are comparable to observations (Figs. 10e,f). It suggests that the origins of the diversity in the amplitudes of the EA center of the PJ pattern in models are different from those of the WNP center. In other words, the SST forcing is not the major cause for the reproducibility of the observed EA center in CMIP5 models.

b. Role of atmospheric mean flow

The PJ pattern is not a pure SST-forced mode, and the maintenance of the PJ pattern involves complex atmospheric internal processes, especially in the middle to high latitudes (Kosaka and Nakamura 2006, 2010). Many studies have demonstrated that the structure and maintenance of some atmospheric teleconnections depend on the configuration of the atmospheric mean flow (e.g., Hoskins and Karoly 1981; Yang and Hoskins 1996; Wang et al. 2018). The strong mean zonal winds such as jets not only act as waveguides along which perturbation energy is allowed to propagate due to the strong meridional gradients of absolute vorticity (Hoskins and Karoly 1981; Branstator 2002), but also facilitate the barotropic energy conversion from the mean flow to eddy due to the strong horizontal wind shear (e.g., Hoskins et al. 1983; Simmons et al. 1983; Kosaka and Nakamura 2006). This mechanism can well explain the formation of some wavelike teleconnections such as the

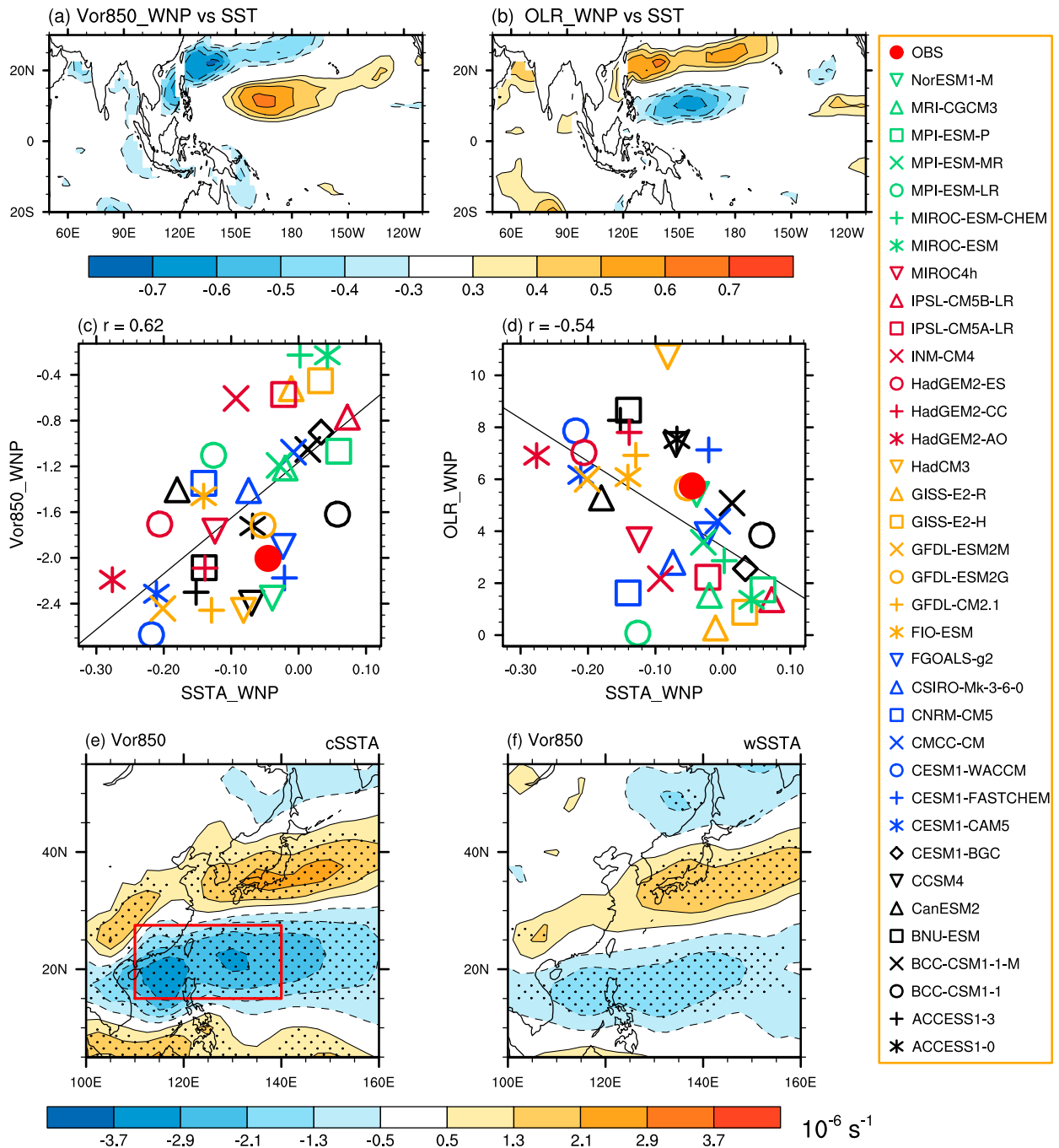


FIG. 10. (a) Intermodel correlation of the area-averaged PJ-index regressed 850-hPa vorticity anomalies over WNP (15° – 27.5° N, 110° – 140° E; Vor850_WNP) with simultaneous PJ-index regressed SSTA in TIP among 36 CMIP5 models. (b) As in (a), but the vorticity is replaced with the area-averaged OLR anomalies over WNP (10° – 22.5° N, 130° – 150° E; OLR_WNP). (c) Scatterplot of the magnitudes of Vor850_WNP (units: 10^{-6} s^{-1} , x axis) with the simultaneous SSTA (units: K, y axis) over WNP (10° – 15° N, 145° – 170° E; SSTA_WNP) (y axis) in each models. (d) As in (c), but for OLR_WNP. (e) The composite PJ pattern in the models with SSTA_WNP < -0.15 K (cSSTA). (f) As in (e), but for the models with SSTA_WNP > 0 K (wSSTA). Dots in (e) and (f) indicate that the anomalies are significant the 90% confidence level based on a two-sided Student's t test.

Silk Road pattern in boreal summer (e.g., Lu et al. 2002; Enomoto et al. 2003; Wang et al. 2017) and the wavelike teleconnections along the subtropical jet in winter (e.g., Branstator 2002; Hu et al. 2017). Since the center of the PJ pattern in the middle and high latitudes cannot be explained by the SST forcing in the tropics, it is worth examining the plausible role of the mean flow (e.g., Lu 2004; Lu and Kim 2004). Note that the PJ pattern is a meridional wave train along the prevailing monsoon southwesterly over the EA in lower troposphere, which is quite different from the teleconnections along the zonal jets. This is because the climatological easterly trade winds are in the eastside of convection anomaly over the WNP, the perturbation energy associated with the PJ pattern cannot propagate in the zonal direction. Kosaka and Nakamura (2006) pointed out that the propagation of the PJ pattern may be primarily through the low-level monsoonal southerlies. On one hand, the prevailing monsoonal southerly serves as a waveguide to allow perturbation energy to propagate poleward; on the other hand, it facilitates the generation of the barotropic energy conversion due to the relative large horizontal wind shear over the EA, helping to maintain the PJ pattern (Kosaka and Nakamura 2006, 2010). Based on the above studies, we propose that the model's reproducibility of the amplitudes in the EA center of the observed PJ pattern may depend on the magnitudes of mean southerly over the coast of EA in the models.

Figure 11a shows the climatology of the 850-hPa meridional winds in the MME during boreal summer. It can be clearly seen that the entire EA region is controlled by southerly flow. The southerly wind is strong from southern China to southeast of Japan (Fig. 11a). This distribution of climatological southerly in the MME is quite similar to that in observations (figure not shown). To investigate the possible link between the mean southerly wind in the EA region and the simulated amplitude of the EA center in the model PJ pattern among CMIP5 models, the amplitudes of the PJ pattern's EA center (Vor850_EA) is defined as the averaged 850-hPa vorticity anomalies over 30°–45°N, 115°–155°E (red box in Fig. 11c) and the intensity of climatological southerly over EA (Clm_V850) is defined as the averaged climatological 850-hPa southerly over 25°–45°N, 115°–155°E (blue box in Fig. 11a). The area of the EA center is fully covered by the area of Clm_V850. Figure 11b presents the scatter diagram of the intensity of Clm_V850 versus Vor850_EA in 36 CMIP5 models and observations. It shows that stronger climatological southerly (i.e., stronger Clm_V850) tends to reproduce larger amplitude of the EA center of the PJ pattern (i.e., larger Vor850_EA) in most of the CMIP5 models. The intermodel correlation coefficient between Clm_V850 and Vor850_EA is 0.5 (Fig. 1a),

exceeding the 99% confidence level (Fig. 11b). It suggests that the reproducibility of the amplitudes of the EA center is indeed closely tied to the intensity of mean meridional wind among CMIP5 models.

To further analyze the effects of mean southerly on the amplitudes of the EA center in models, six models with strongest southerly (SV850) and six models with weakest southerly (WV850) are selected for comparison. Figures 11c and 11d show the composite PJ pattern in the SV850 and WV850 models, respectively. In SV850 models, a pronounced meridional tripole pattern with zonally elongated vorticity anomalies is observed over EA-WNP, accompanied by evident poleward wave-activity fluxes in the lower troposphere (Fig. 11c). In WV850 models, in contrast, the magnitude of the EA center is much weaker than that in SV850 models, accompanied by very weak wave-activity fluxes over EA-WNP (Fig. 11d). Meanwhile, the intermodel correlation coefficient between the ratio of the vorticity anomalies in the EA center to that in the WNP center, and the climatological southerly over the EA reaches 0.37, exceeding the 95% confidence level. These results suggest that strong climatological southerly over EA indeed facilitates the northward propagation of the PJ pattern and large amplitude of the EA center of the PJ pattern in models. In addition, the center north of Japan is also very weak in WV850 models compared with that in SV850 models (Figs. 11c,d). The intermodel correlation between Clm_V850 and the north center defined as the area-averaged vorticity anomalies over 45°–60°N, 130°–160°E is –0.28, reaching the 90% confidence level. This feature further suggests that the poleward propagation of wave-activity fluxes tied to the mean southerly is very important in the formation of the centers of middle and high latitudes in the model PJ pattern in the CMIP5 models.

Meanwhile, it is noted that the absolute magnitude of the EA center is the strongest among three centers of the PJ pattern in SV850 models. Therefore, the amplitude of the EA center may not only be related to the energy dispersion from the tropical center, but also may be attributed to the nonlinear interactions between the mean flow and anomalies over EA. To illustrate the effect of the interactions between the mean flow and anomalies on the amplitudes of the EA center in detail, the local barotropic energy conversion (CK) associated with the PJ pattern is estimated in the SV850 and WV850 models. The evaluation is based on the following formula (e.g., Hoskins et al. 1983; Simmons et al. 1983; Kosaka and Nakamura 2006):

$$CK = \frac{v'^2 - u'^2}{2} \left(\frac{\partial \bar{u}}{\partial x} - \frac{\partial \bar{v}}{\partial y} \right) - u'v' \left(\frac{\partial \bar{u}}{\partial y} + \frac{\partial \bar{v}}{\partial x} \right).$$

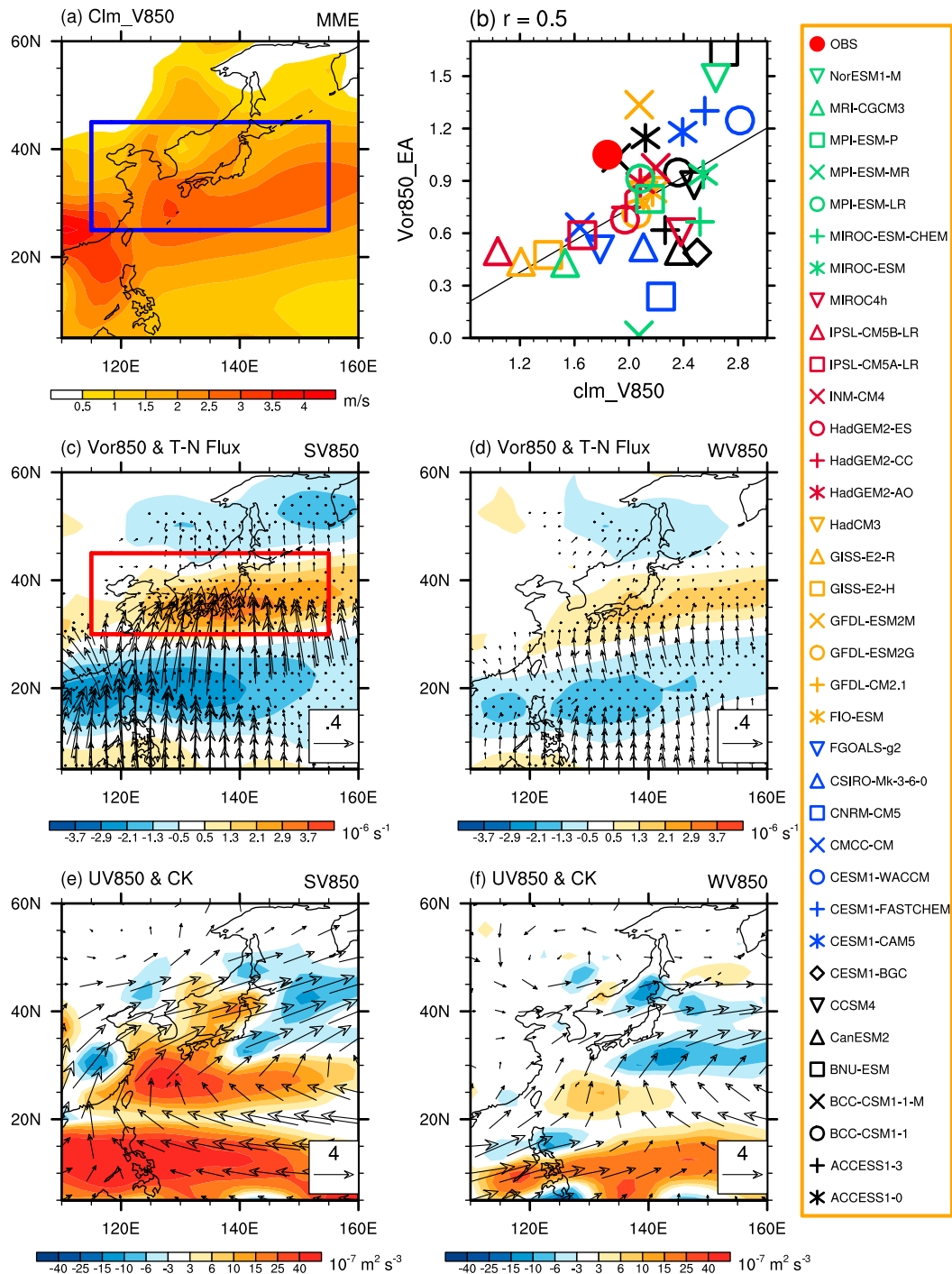


FIG. 11. (a) The MME (shading) of climatological 850-hPa meridional wind during boreal summer in 36 CMIP5 models. (b) Scatterplot of the averaged climatological 850-hPa meridional wind (units: $m s^{-1}$; x axis) over the coast of EA (25° – 45° N, 115° – 155° E) with the 850-hPa vorticity anomalies (units: $10^{-6} s^{-1}$; y axis) over EA (30° – 45° N, 115° – 155° E) in 36 CMIP5 models. (c),(d) PJ-related 850-hPa vorticity and wave-activity fluxes in the six models with strongest and weakest climatological 850-hPa meridional wind, respectively. (e),(f) Climatological 850-hPa wind vectors and model PJ-related barotropic energy conversion (CK, units: $10^{-7} m^2 s^{-3}$). Dots in (c) and (d) indicate the 90% confidence level of shading based on a two-sided Student's t test.

Here, positive CK means conversion of kinetic energy from the mean flow to the anomalies associated with the PJ pattern. The climatological 850-hPa southerlies are much stronger over the coast of the EA in the SV850 models than those in the WV850 models, and the horizontal wind shears are also larger over the EA in the SV850 models than those in the WV850 models (Figs. 11e,f). Accordingly, there are more local barotropic energy conversions from mean southerly to the PJ pattern over the coast of EA in the SV850 models than in the WV850 models (Figs. 11e,f), which indicates the positive effect of CK on strengthening and maintaining the EA center of the PJ pattern in the SV850 models. To further quantify the effect of the barotropic energy conversion, the time scale (τ_{CK}) with which the perturbation kinetic energy [$KE = (u'^2 + v'^2)/2$] could be fully replenished through CK is calculated:

$$\tau_{CK} = \frac{\langle KE \rangle}{\langle CK \rangle},$$

where the brackets represent a horizontal integral over the entire latitudinal band between 5° and 85°N. The calculated τ_{CK} is 16.98 days and 29.72 days in the SV850 and WV850 models, respectively, indicating that CK is more effective at maintaining the PJ pattern in the SV850 models than in WV850 models. Note that although CK is determined by both the PJ-related anomalies and the magnitudes of mean flow, τ_{CK} only depends on the mean flow if the PJ-related anomaly structure is fixed. In other words, when the structures of the mean flow and the PJ pattern are fixed, increases in the magnitude of the PJ pattern do not change the efficiency of the barotropic process to maintain the PJ pattern (i.e., τ_{CK}). In contrast, increases in the magnitude of the mean flow can reduce τ_{CK} . Therefore, the barotropic energy conversion to maintain the PJ pattern is more efficient in SV850 models than in WV850 models due to its stronger mean flow. In addition to the strength, the structure of the mean flow also influences the efficiency of barotropic energy conversion, but this effect is difficult to measure at this stage and will be investigated in our future studies. To sum up, the above results suggest that the strong climatological monsoonal southerlies over the coast of EA not only facilitate the propagation of the PJ-related vorticity anomalies from tropics to the middle latitudes, but also strengthen and maintain the PJ pattern due to the strong local barotropic energy conversion over the EA.

5. Summary and discussion

In this study, the intermodel diversity of the PJ pattern in boreal summer are investigated in 36 CMIP5 models

with an emphasis on the pattern's structure and amplitude. Since the dominant mode of the climate variability over the summertime WNP is the PJ pattern in observations, the leading modes extracted as a linear combination of EOF1 and EOF2 in the 850 hPa vorticity anomalies over the WNP are employed and named as the model PJ pattern to investigate the model's reproducibility of the observed PJ pattern. The model's reproducibility of the spatial structure of the observed PJ pattern is measured by the pattern correlation between the simulated and observed PJ patterns. In observations, the PJ pattern is characterized by a meridional wave pattern with zonally elongated anticyclonic, cyclonic, and anticyclonic vorticity anomalies in the lower troposphere over EA-WNP. The MME reproduces well the meridional tripole of vorticity anomalies over EA-WNP, but the magnitudes are generally weaker than those in observations. Based on the spatial similarity of the PJ pattern between models and observations, a composite analysis is conducted to further show the differences of the spatial structure of the model PJ pattern in detail among models. The spatial structure of the model PJ pattern, and associated OLR, circulation, and rainfall pattern are well reproduced in the HCG models, whereas they are not well organized in the LCG models.

Since the observed PJ pattern is largely forced by the tropical SSTA due to the close relationship with convection anomaly over the WNP, the role of the SSTA pattern is analyzed to explain the diversity of the model's reproducibility of spatial structure of the observed PJ pattern. It reveals that the realistic convection anomaly over the WNP and the spatial structure of the PJ pattern are reproduced if significant warm (cold) SSTA is observed in the TIO (WNP and central Pacific) in CMIP5 models. Furthermore, the cold SSTAs in the WNP and central Pacific play a very important role in reproducing the spatial structure of the PJ pattern in the models, whereas the effect of TIO SSTAs is underestimated, suggesting that the positive thermodynamic air-sea interaction in the WNP is important for the model reproducibility of the observed PJ in those models. However, the reasons for the strong positive local air-sea interaction in the WNP during boreal summer are not clear and need to be further investigated. Meanwhile, the simultaneous SSTAs are found to be closely tied to the preceding ENSO-related SSTA pattern and its temporal evolution in the tropical Indo-Pacific Ocean in both observations and models. And the observed PJ pattern could be well reproduced if the ENSO SSTA in preceding winter is well captured in most of models, suggesting the importance of the simulation of ENSO in the reproducibility of the observed PJ pattern in CMIP5 models.

Moreover, the model's reproducibility of the amplitudes of WNP and EA centers are further examined. Results show that the diverse reproducibility of the amplitudes of the observed WNP center is closely tied to the cold SSTA in the WNP in models. The positive local air-sea feedback in the WNP facilitates the formation and maintenance of the WNP center of the model PJ pattern, thereby reproducing a realistic PJ pattern in models. Meanwhile, the model reproducibility of the amplitudes of EA center in the observed PJ pattern is found to be associated with the atmospheric mean flow over the coast of the EA in the models. With the intensification of the mean southerly, there are stronger poleward wave-activity flux from lower latitudes to middle and high latitudes, indicating effective energy dispersion from the tropics to the middle and high latitudes. This process is important for the formation of the EA center in models. Meanwhile, the effective barotropic energy conversion caused by large horizontal wind shear associated with the strong climatological monsoonal southerly can also strengthen the EA center of the PJ pattern due to the more efficient local barotropic energy conversion from the mean flow. It suggests that the model's reproducibility of the amplitude of EA center is largely determined by the magnitude of atmospheric mean flow over the EA in models.

Although the role of the mean flow is analyzed based on the southerly winds, the conclusions also hold if the magnitude of the southwesterly monsoonal winds is used. This is because the magnitude of the climatological southerly winds reflects that of the climatological southwesterly winds to much extent (Figs. 11e,f). In fact, we used the magnitudes of climatological southwesterlies at 850 hPa to define SV850 and WV850 models and repeated the analyses in section 4b. The results remain almost the same with slightly weaker signals (not shown). We infer that this is because the same magnitude of winds can correspond to different wind directions, and that the pattern of the mean flow is also important for the simulation of the PJ pattern in models as discussed in section 4b. Compared with the magnitude of the wind vectors, the magnitude of meridional winds may be a simpler and better metric to measure the role of the mean flow in models.

The results of this study suggest that improvement of models in the simulation of the ENSO SSTA pattern and the simultaneous SSTAs in TIP, as well with the atmospheric mean flow over EA, can help to reproduce a more realistic PJ pattern. The barotropic energy conversion is emphasized when the role of the mean flow is discussed. Nevertheless, the baroclinic energy conversion is also important to maintain the PJ

pattern (Kosaka and Nakamura 2006), and how it contributes to the diversity of the simulated PJ pattern in models need be explored in the future. Last but not least, the north center of the PJ pattern is generally weaker in models than that in observations. Since the north center of the PJ pattern is located in the mid and high latitudes where the atmospheric processes are more chaotic than those in the low latitudes, it may be difficult to be well reproduced by the current climate models. The possible factors responsible for the amplitudes of the north center also need to be investigated in the future.

Acknowledgments. We are very grateful to the three anonymous reviewers and the editor Hisashi Nakamura for their insightful comments that helped to improve the manuscript. We acknowledge the climate modeling groups (listed in section 2) for producing and making available their model output. For CMIP the U.S. Department of Energy's Program for Climate Model Diagnosis and Intercomparison provided coordinating support and led development of software infrastructure in partnership with the Global Organization for Earth System Science Portals. This work was supported by the National Key R&D Program of China (2016YFA0600600), the National Natural Science Foundation of China (41661144016, and 41605060), and the Fundamental Research Funds for the Central Universities.

REFERENCES

- Barsugli, J. J., and P. D. Sardeshmukh, 2002: Global atmospheric sensitivity to tropical SST anomalies throughout the Indo-Pacific basin. *J. Climate*, **15**, 3427–3442, [https://doi.org/10.1175/1520-0442\(2002\)015<3427:GASTTS>2.0.CO;2](https://doi.org/10.1175/1520-0442(2002)015<3427:GASTTS>2.0.CO;2).
- Branstator, G., 2002: Circumglobal teleconnections, the jet stream waveguide, and the North Atlantic Oscillation. *J. Climate*, **15**, 1893–1910, [https://doi.org/10.1175/1520-0442\(2002\)015<1893:CTTJSW>2.0.CO;2](https://doi.org/10.1175/1520-0442(2002)015<1893:CTTJSW>2.0.CO;2).
- Chen, X., and T. Zhou, 2014: Relative role of tropical SST forcing in the 1990s periodicity change of the Pacific–Japan pattern interannual variability. *J. Geophys. Res. Atmos.*, **119**, 13 043–13 066, <https://doi.org/10.1002/2014JD022064>.
- Chen, W., J.-Y. Lee, K.-J. Ha, K.-S. Yun, and R. Lu, 2016: Intensification of the western North Pacific anticyclone response to the short decaying El Niño event due to greenhouse warming. *J. Climate*, **29**, 3607–3627, <https://doi.org/10.1175/JCLI-D-15-0195.1>.
- Chen, Z., Z. Wen, R. Wu, X. Lin, and J. Wang, 2016: Relative importance of tropical SST anomalies in maintaining the western North Pacific anomalous anticyclone during El Niño to La Niña transition years. *Climate Dyn.*, **46**, 1027–1041, <https://doi.org/10.1007/s00382-015-2630-1>.
- , —, —, and Y. Du, 2017: Roles of tropical SST anomalies in modulating the western north Pacific anomalous cyclone during strong La Niña decaying years. *Climate Dyn.*, **49**, 633–647, <https://doi.org/10.1007/s00382-016-3364-4>.

- Chowdary, J. S., S.-P. Xie, J.-J. Luo, J. Hafner, S. Behera, Y. Masumoto, and T. Yamagata, 2011: Predictability of Northwest Pacific climate during summer and the role of the tropical Indian Ocean. *Climate Dyn.*, **36**, 607–621, <https://doi.org/10.1007/s00382-009-0686-5>.
- , —, H. Tokinaga, Y. M. Okumura, H. Kubota, N. Johnson, and X.-T. Zheng, 2012: Interdecadal variations in ENSO teleconnection to the Indo-western Pacific for 1870–2007. *J. Climate*, **25**, 1722–1744, <https://doi.org/10.1175/JCLI-D-11-00070.1>.
- , C. Gnanaseelan, and S. Chakravorty, 2013: Impact of northwest Pacific anticyclone on the Indian summer monsoon region. *Theor. Appl. Climatol.*, **113**, 329–336, <https://doi.org/10.1007/s00704-012-0785-9>.
- , H. S. Harsha, C. Gnanaseelan, G. Srinivas, A. Parekh, P. A. Pillai, and C. V. Naidu, 2017: Indian summer monsoon rainfall variability in response to differences in the decay phase of El Niño. *Climate Dyn.*, **48**, 2707–2727, <https://doi.org/10.1007/s00382-016-3233-1>.
- Dee, D. P., and Coauthors, 2011: The ERA-interim reanalysis: Configuration and performance of the data assimilation system. *Quart. J. Roy. Meteor. Soc.*, **137**, 553–597, <https://doi.org/10.1002/qj.828>.
- Ding, H., R. Greatbatch, W. Park, M. Latif, V. Semenov, and X. Sun, 2014: The variability of the East Asian summer monsoon and its relationship to ENSO in a partially coupled climate model. *Climate Dyn.*, **42**, 367–379, <https://doi.org/10.1007/s00382-012-1642-3>.
- Enomoto, T., B. J. Hoskins, and Y. Matsuda, 2003: The formation mechanism of the Bonin high in August. *Quart. J. Roy. Meteor. Soc.*, **129**, 157–178, <https://doi.org/10.1256/qj.01.211>.
- Gao, H., S. Yang, A. Kumar, Z.-Z. Hu, B. Huang, Y. Li, and B. Jha, 2011: Variations of the East Asian mei-yu and simulation and prediction by the NCEP Climate Forecast System. *J. Climate*, **24**, 94–108, <https://doi.org/10.1175/2010JCLI3540.1>.
- Gong, H., L. Wang, W. Chen, R. Wu, K. Wei, and X. Cui, 2014: The climatology and interannual variability of the East Asian winter monsoon in CMIP5 models. *J. Climate*, **27**, 1659–1678, <https://doi.org/10.1175/JCLI-D-13-00039.1>.
- , —, —, D. Nath, G. Huang, and W. Tao, 2015: Diverse influences of ENSO on the East Asian–western Pacific winter climate tied to different ENSO properties in CMIP5 models. *J. Climate*, **28**, 2187–2202, <https://doi.org/10.1175/JCLI-D-14-00405.1>.
- , —, —, X. Chen, and D. Nath, 2017: Biases of the wintertime Arctic Oscillation in CMIP5 models. *Environ. Res. Lett.*, **12**, 014001, <https://doi.org/10.1088/1748-9326/12/1/014001>.
- Gong, Z., G. Feng, M. Dogar, and G. Huang, 2017: The possible physical mechanism for the EAP-SR co-action. *Climate Dyn.*, <https://doi.org/10.1007/s00382-017-3967-4>.
- He, C., and T. Zhou, 2014: The two interannual variability modes of the western North Pacific subtropical high simulated by 28 CMIP5-AMIP models. *Climate Dyn.*, **43**, 2455–2469, <https://doi.org/10.1007/s00382-014-2068-x>.
- Hoskins, B. J., and D. Karoly, 1981: The steady linear response of a spherical atmosphere to thermal and orographic forcing. *J. Atmos. Sci.*, **38**, 1179–1196, [https://doi.org/10.1175/1520-0469\(1981\)038<1179:TSLROA>2.0.CO;2](https://doi.org/10.1175/1520-0469(1981)038<1179:TSLROA>2.0.CO;2).
- , I. N. James, and G. H. White, 1983: The shape, propagation, and mean-flow interaction of large-scale weather systems. *J. Atmos. Sci.*, **40**, 1595–1612, [https://doi.org/10.1175/1520-0469\(1983\)040<1595:TSPAMF>2.0.CO;2](https://doi.org/10.1175/1520-0469(1983)040<1595:TSPAMF>2.0.CO;2).
- Hu, K., G. Huang, R. Wu, and L. Wang, 2017: Structure and dynamics of a wave train along the wintertime Asian jet and its impact on East Asian climate. *Climate Dyn.*, <https://doi.org/10.1007/s00382-017-3674-1>.
- Huang, R., and F. Sun, 1992: Impact of the tropical western Pacific on the East Asian summer monsoon. *J. Meteor. Soc. Japan*, **70**, 243–256, https://doi.org/10.2151/jmsj1965.70.1B_243.
- , J. Chen, L. Wang, and Z. Lin, 2012: Characteristics, processes, and causes of the spatio-temporal variabilities of the East Asian monsoon system. *Adv. Atmos. Sci.*, **29**, 910–942, <https://doi.org/10.1007/s00376-012-2015-x>.
- Huffman, G. J., R. F. Adler, D. T. Bolvin, and G. J. Gu, 2009: Improving the global precipitation record: GPCP version 2.1. *Geophys. Res. Lett.*, **36**, L17808, <https://doi.org/10.1029/2009GL040000>.
- Jiang, W., G. Huang, K. Hu, R. Wu, H. Gong, X. Chen, and W. Tao, 2017: Diverse relationship between ENSO and the Northwest Pacific summer climate among CMIP5 models: Dependence on the ENSO decay pace. *J. Climate*, **30**, 109–127, <https://doi.org/10.1175/JCLI-D-16-0365.1>.
- Jiang, X., S. Yang, Y. Li, A. Kumar, X. Liu, Z. Zuo, and B. Jha, 2013: Seasonal-to-interannual prediction of the Asian summer monsoon in the NCEP Climate Forecast System version 2. *J. Climate*, **26**, 3708–3727, <https://doi.org/10.1175/JCLI-D-12-00437.1>.
- Kosaka, Y., and H. Nakamura, 2006: Structure and dynamics of the summertime Pacific–Japan teleconnection pattern. *Quart. J. Roy. Meteor. Soc.*, **132**, 2009–2030, <https://doi.org/10.1256/qj.05.204>.
- , and —, 2010: Mechanisms of meridional teleconnection observed between a summer monsoon system and a subtropical anticyclone. Part I: The Pacific–Japan pattern. *J. Climate*, **23**, 5085–5108, <https://doi.org/10.1175/2010JCLI3413.1>.
- , and —, 2011: Dominant mode of climate variability, intermodel diversity, and projected future changes over the summertime western North Pacific simulated in the CMIP3 models. *J. Climate*, **24**, 3935–3955, <https://doi.org/10.1175/2011JCLI3907.1>.
- , J. S. Chowdary, S.-P. Xie, Y.-M. Min, and J.-Y. Lee, 2012: Limitations of seasonal predictability for summer climate over East Asia and the Northwestern Pacific. *J. Climate*, **25**, 7574–7589, <https://doi.org/10.1175/JCLI-D-12-00009.1>.
- Kubota, H., Y. Kosaka, and S.-P. Xie, 2016: A 117-year long index of the Pacific–Japan pattern with application to interdecadal variability. *Int. J. Climatol.*, **36**, 1575–1589, <https://doi.org/10.1002/joc.4441>.
- Lee, E., S. Yeh, J. Jhun, and B. Moon, 2006: Seasonal change in anomalous WNPSH associated with the strong East Asian summer monsoon. *Geophys. Res. Lett.*, **33**, L21702, <https://doi.org/10.1029/2006GL027474>.
- Li, C., R. Lu, and B. Dong, 2012: Predictability of the western North Pacific summer climate demonstrated by the coupled models of ENSEMBLES. *Climate Dyn.*, **39**, 329–346, <https://doi.org/10.1007/s00382-011-1274-z>.
- Li, R. C. Y., W. Zhou, and T. Li, 2014: Influences of the Pacific–Japan teleconnection pattern on synoptic-scale variability in the western North Pacific. *J. Climate*, **27**, 140–154, <https://doi.org/10.1175/JCLI-D-13-00183.1>.
- Li, T., and B. Wang, 2005: A review on the western North Pacific monsoon: Synoptic-to-interannual variability. *Terr. Atmos. Ocean. Sci.*, **16**, 285–314, [https://doi.org/10.3319/TAO.2005.16.2.285\(A\)](https://doi.org/10.3319/TAO.2005.16.2.285(A)).

- , —, and L. Wang, 2016: Comments on “Combination mode dynamics of the anomalous northwest Pacific anticyclone.” *J. Climate*, **29**, 4685–4693, <https://doi.org/10.1175/JCLI-D-15-0385.1>.
- , —, B. Wu, T. Zhou, C.-P. Chang, and R. Zhang, 2017: Theories on formation of an anomalous anticyclone in western North Pacific during El Niño: A review. *J. Meteor. Res.*, **31**, 987–1006, <https://doi.org/10.1007/s13351-017-7147-6>.
- Liebmann, B., and C. A. Smith, 1996: Description of a complete (interpolated) outgoing longwave radiation dataset. *Bull. Amer. Meteor. Soc.*, **77**, 1275–1277.
- Lu, R., 2004: Associations among the components of the East Asian summer monsoon system in the meridional direction. *J. Meteor. Soc. Japan*, **82**, 155–165, <https://doi.org/10.2151/jmsj.82.155>.
- , and B. Kim, 2004: The climatological Rossby wave source over the STCZs in the summer Northern Hemisphere. *J. Meteor. Soc. Japan*, **82**, 657–669, <https://doi.org/10.2151/jmsj.2004.657>.
- , J.-H. Oh, and B.-J. Kim, 2002: A teleconnection pattern in upper-level meridional wind over the North African and Eurasian continent in summer. *Tellus*, **54A**, 44–55, <https://doi.org/10.3402/tellusa.v54i1.12122>.
- , Y. Li, and B. Dong, 2006: External and internal summer atmospheric variability in the western North Pacific and East Asia. *J. Meteor. Soc. Japan*, **84**, 447–462, <https://doi.org/10.2151/jmsj.84.447>.
- Nakamura, H., and T. Fukamachi, 2004: Evolution and dynamics of summertime blocking over the Far East and the associated surface Okhotsk high. *Quart. J. Roy. Meteor. Soc.*, **130**, 1213–1233, <https://doi.org/10.1256/qj.03.101>.
- Nitta, T., 1987: Convective activities in the tropical western Pacific and their impact on the Northern Hemisphere summer circulation. *J. Meteor. Soc. Japan*, **65**, 373–390, https://doi.org/10.2151/jmsj1965.65.3_373.
- North, G. R., T. L. Bell, R. F. Cahalan, and F. J. Moeng, 1982: Sampling errors in the estimation of empirical orthogonal functions. *Mon. Wea. Rev.*, **110**, 699–706, [https://doi.org/10.1175/1520-0493\(1982\)110<0699:SEITEO>2.0.CO;2](https://doi.org/10.1175/1520-0493(1982)110<0699:SEITEO>2.0.CO;2).
- Ramu, D. A., J. S. Chowdary, S. S. V. S. Ramakrishna, and O. S. R. U. B. Kumar, 2018: Diversity in the representation of large-scale circulation associated with ENSO-Indian summer monsoon teleconnections in CMIP5 models. *Theor. Appl. Climatol.*, **132**, 465–478, <https://doi.org/10.1007/s00704-017-2092-y>.
- Simmons, A. J., J. M. Wallace, and G. W. Branstator, 1983: Barotropic wave propagation and instability, and atmospheric teleconnection patterns. *J. Atmos. Sci.*, **40**, 1363–1392, [https://doi.org/10.1175/1520-0469\(1983\)040<1363:BWPAIA>2.0.CO;2](https://doi.org/10.1175/1520-0469(1983)040<1363:BWPAIA>2.0.CO;2).
- Smith, T. M., R. W. Reynolds, T. C. Peterson, and J. Lawrimore, 2008: Improvements to NOAA’s historical merged land-ocean surface temperature analysis (1880–2006). *J. Climate*, **21**, 2283–2296, <https://doi.org/10.1175/2007JCLI2100.1>.
- Song, F., and T. Zhou, 2014a: Interannual variability of East Asian summer monsoon simulated by CMIP3 and CMIP5 AGCMs: Skill dependence on Indian Ocean–western Pacific anticyclone teleconnection. *J. Climate*, **27**, 1679–1697, <https://doi.org/10.1175/JCLI-D-13-00248.1>.
- , and —, 2014b: The climatology and interannual variability of East Asian summer monsoon in CMIP5 coupled models: Does air–sea coupling improve the simulations? *J. Climate*, **27**, 8761–8777, <https://doi.org/10.1175/JCLI-D-14-00396.1>.
- Srinivas, G., J. S. Chowdary, Y. Kosaka, C. Gnanaseelan, A. Parekh, and K. V. S. R. Prasad, 2018: Influence of the Pacific–Japan pattern on Indian summer monsoon rainfall. *J. Climate*, **31**, 3943–3958, <https://doi.org/10.1175/JCLI-D-17-0408.1>.
- Takaya, K., and H. Nakamura, 2001: A formulation of a phase-independent wave-activity flux for stationary and migratory quasigeostrophic eddies on a zonally varying basic flow. *J. Atmos. Sci.*, **58**, 608–627, [https://doi.org/10.1175/1520-0469\(2001\)058<0608:AFOAPI>2.0.CO;2](https://doi.org/10.1175/1520-0469(2001)058<0608:AFOAPI>2.0.CO;2).
- Tao, W., G. Huang, K. Hu, H. Gong, G. Wen, and L. Liu, 2016: A study of biases in simulation of the Indian Ocean basin mode and its capacitor effect in CMIP3/CMIP5 models. *Climate Dyn.*, **46**, 205–226, <https://doi.org/10.1007/s00382-015-2579-0>.
- Taylor, K. E., R. J. Stouffer, and G. A. Meehl, 2012: An overview of CMIP5 and the experiment design. *Bull. Amer. Meteor. Soc.*, **93**, 485–498, <https://doi.org/10.1175/BAMS-D-11-00094.1>.
- Wang, B., R. Wu, and X. Fu, 2000: Pacific–East Asian teleconnection: How does ENSO affect East Asian climate? *J. Climate*, **13**, 1517–1536, [https://doi.org/10.1175/1520-0442\(2000\)013<1517:PEATHD>2.0.CO;2](https://doi.org/10.1175/1520-0442(2000)013<1517:PEATHD>2.0.CO;2).
- , —, and K. Lau, 2001: Interannual variability of the Asian summer monsoon: Contrasts between the Indian and the western North Pacific–East Asian monsoon. *J. Climate*, **14**, 4073–4090, [https://doi.org/10.1175/1520-0442\(2001\)014<4073:IVOTAS>2.0.CO;2](https://doi.org/10.1175/1520-0442(2001)014<4073:IVOTAS>2.0.CO;2).
- , —, and T. Li, 2003: Atmosphere–warm ocean interaction and its impacts on Asian–Australian monsoon variation. *J. Climate*, **16**, 1195–1211, [https://doi.org/10.1175/1520-0442\(2003\)16<1195:AOIAII>2.0.CO;2](https://doi.org/10.1175/1520-0442(2003)16<1195:AOIAII>2.0.CO;2).
- , B. Xiang, and J.-Y. Lee, 2013: Subtropical high predictability establishes a promising way for monsoon and tropical storm predictions. *Proc. Natl. Acad. Sci. USA*, **110**, 2718–2722, <https://doi.org/10.1073/pnas.1214626110>.
- Wang, J., Z. Wen, R. Wu, Y. Guo, and Z. Chen, 2016: The mechanism of growth of the low-frequency East Asia–Pacific teleconnection and the triggering role of tropical intraseasonal oscillation. *Climate Dyn.*, **46**, 3965–3977, <https://doi.org/10.1007/s00382-015-2815-7>.
- Wang, L., P. Xu, W. Chen, and Y. Liu, 2017: Interdecadal variations of the Silk Road pattern. *J. Climate*, **30**, 9915–9932, <https://doi.org/10.1175/JCLI-D-17-0340.1>.
- , Y. Y. Liu, Y. Zhang, W. Chen, and S. F. Chen, 2018: Time-varying structure of the wintertime Eurasian pattern: Role of the North Atlantic sea surface temperature and atmospheric mean flow. *Climate Dyn.*, <https://doi.org/10.1007/s00382-018-4261-9>.
- Wu, B., T. Li, and T. Zhou, 2010: Relative contributions of the Indian Ocean and local SST anomalies to the maintenance of the western North Pacific anomalous anticyclone during El Niño decaying summer. *J. Climate*, **23**, 2974–2986, <https://doi.org/10.1175/2010JCLI3300.1>.
- Wu, R., and B. Wang, 2000: Interannual variability of summer monsoon onset over the western North Pacific and the underlying processes. *J. Climate*, **13**, 2483–2501, [https://doi.org/10.1175/1520-0442\(2000\)013<2483:IVOSMO>2.0.CO;2](https://doi.org/10.1175/1520-0442(2000)013<2483:IVOSMO>2.0.CO;2).
- , and —, 2002: A contrast of the East Asian summer monsoon–ENSO relationship between 1962–77 and 1978–93. *J. Climate*, **15**, 3266–3279, [https://doi.org/10.1175/1520-0442\(2002\)015<3266:ACOTEA>2.0.CO;2](https://doi.org/10.1175/1520-0442(2002)015<3266:ACOTEA>2.0.CO;2).
- , Z.-Z. Hu, and B. P. Kirtman, 2003: Evolution of ENSO-related rainfall anomalies in East Asia. *J. Climate*, **16**, 3742–3758, [https://doi.org/10.1175/1520-0442\(2003\)016<3742:EOERAI>2.0.CO;2](https://doi.org/10.1175/1520-0442(2003)016<3742:EOERAI>2.0.CO;2).
- , G. Huang, Z. Du, and K. Hu, 2014: Cross-season relation of the South China Sea precipitation variability between winter

- and summer. *Climate Dyn.*, **43**, 193–207, <https://doi.org/10.1007/s00382-013-1820-y>.
- Xiang, B., B. Wang, W. Yu, and S. Xu, 2013: How can anomalous western North Pacific subtropical high intensify in late summer? *Geophys. Res. Lett.*, **40**, 2349–2354, <https://doi.org/10.1002/grl.50431>.
- Xie, S.-P., K. Hu, J. Hafner, H. Tokinaga, Y. Du, G. Huang, and T. Sampe, 2009: Indian Ocean capacitor effect on Indo-western Pacific climate during the summer following El Niño. *J. Climate*, **22**, 730–747, <https://doi.org/10.1175/2008JCLI2544.1>.
- , Y. Du, G. Huang, X.-T. Zheng, H. Tokinaga, K. Hu, and Q. Liu, 2010: Decadal shift in El Niño influences on Indo-western Pacific and East Asian climate in the 1970s. *J. Climate*, **23**, 3352–3368, <https://doi.org/10.1175/2010JCLI3429.1>.
- , Y. Kosaka, Y. Du, K. Hu, J. S. Chowdary, and G. Huang, 2016: Indo-western Pacific Ocean capacitor and coherent climate anomalies in post-ENSO summer: A review. *Adv. Atmos. Sci.*, **33**, 411–432, <https://doi.org/10.1007/s00376-015-5192-6>.
- Yang, G.-Y., and B. J. Hoskins, 1996: Propagation of Rossby waves of nonzero frequency. *J. Atmos. Sci.*, **53**, 2365–2378, [https://doi.org/10.1175/1520-0469\(1996\)053<2365:PORWON>2.0.CO;2](https://doi.org/10.1175/1520-0469(1996)053<2365:PORWON>2.0.CO;2).
- Yang, J., Q. Liu, S.-P. Xie, Z. Liu, and L. Wu, 2007: Impact of the Indian Ocean SST basin mode on the Asian summer monsoon. *Geophys. Res. Lett.*, **34**, L02708, <https://doi.org/10.1029/2006GL028571>.
- Yang, S., and X. Jiang, 2014: Prediction of eastern and central Pacific ENSO events and their impacts on East Asian climate by the NCEP Climate Forecast System. *J. Climate*, **27**, 4451–4472, <https://doi.org/10.1175/JCLI-D-13-00471.1>.
- , K.-M. Lau, and M. Sankar-Rao, 1996: Precursory signals associated with the interannual variability of the Asian summer monsoon. *J. Climate*, **9**, 949–964, [https://doi.org/10.1175/1520-0442\(1996\)009<0949:PSAWTI>2.0.CO;2](https://doi.org/10.1175/1520-0442(1996)009<0949:PSAWTI>2.0.CO;2).
- , Z. Zhang, V. E. Kousky, R. W. Higgins, S.-H. Yoo, J. Liang, and Y. Fan, 2008: Simulations and seasonal prediction of the Asian summer monsoon in the NCEP Climate Forecast System. *J. Climate*, **21**, 3755–3775, <https://doi.org/10.1175/2008JCLI1961.1>.
- Zhang, R., A. Sumi, and M. Kimoto, 1996: Impact of El Niño on the East Asian monsoon: A diagnostic study of the '86/87 and '91/92 events. *J. Meteor. Soc. Japan*, **74**, 49–62, https://doi.org/10.2151/jmsj1965.74.1_49.
- , —, and —, 1999: A diagnostic study of the impact of El Niño on the precipitation in China. *Adv. Atmos. Sci.*, **16**, 229–241, <https://doi.org/10.1007/BF02973084>.
- , Q. Min, and J. Su, 2017: Impact of El Niño on atmospheric circulations over East Asia and rainfall in China: Role of the anomalous western North Pacific anticyclone. *Sci. China Earth Sci.*, **60**, 1124–1132, <https://doi.org/10.1007/s11430-016-9026-x>.
- Zhao, G., G. Huang, R. Wu, W. Tao, H. Gong, X. Qu, and K. Hu, 2015: A new upper-level circulation index for the East Asian summer monsoon variability. *J. Climate*, **28**, 9977–9996, <https://doi.org/10.1175/JCLI-D-15-0272.1>.